

1 **Observations of the temporal variability in aerosol properties and their relationships to**
2 **meteorology in the summer monsoonal South China Sea/East Sea: The scale-dependent**
3 **role of monsoonal flows, the Madden-Julian Oscillation, tropical cyclones, squall lines and**
4 **cold pools.**
5

6 Jeffrey S. Reid¹, Nofel D. Lagrosas², Haflidi H. Jonsson³, Elizabeth A. Reid¹, Walter R.
7 Sessions⁴, James B. Simpas²; Sherdon N. Uy², Thomas J. Boyd⁵; Samuel A. Atwood⁶; Donald
8 R. Blake⁷, James R. Campbell¹, Steven S. Cliff⁸, Brent N. Holben⁹, Robert E. Holz¹⁰, Edward J.
9 Hyer¹, Peng Lynch¹¹, Simone Meinardi⁷, Derek J. Posselt¹², Kim A. Richardson¹, Santo V.
10 Salinas¹³, Alexander Smirnov¹⁴, Qing Wang³, Liya Yu¹⁵, Jianglong Zhang¹⁶.

11
12 [1] {Marine Meteorology Division, Naval Research Laboratory, Monterey CA}

13 [2] {

14 Manila Observatory, Ateneo de Manila University, Quezon City, Philippines

15 }

16 [3] {Department of Meteorology, Naval Postgraduate School, Monterey CA}

17 [4] {CSC, Naval Research Laboratory, Monterey CA}

18 [5] {Biogeochemistry Section, Naval Research Laboratory, Washington DC}

19 [6] {Dept. of Atmospheric Science, Colorado State University, Ft. Collins, CO}

20 [7] {University of California, Irvine, CA}

21 [8] {University of California, Davis, CA}

22 [9] {NASA Goddard Space Flight Center}

23 [10] {Space Sciences Engineering Center, University of Wisconsin, Madison, WI}

24 [11] {CSC Inc. at Naval Research Laboratory, Monterey CA}

25 [12] {Dept. of Atmospheric, Oceanic, and Space Sciences, University of Michigan, Ann Arbor,
26 MI}

27 [13] {Centre for Remote Imaging Sensing and Processing, National University
28 of Singapore, Singapore}

29 [14] {Sigma Space Corporation, Lanham, MD}

30 [15] {Dept. of environmental Engineering, National University of Singapore, Singapore}

31 {National University of Singapore, Singapore}

32 [16] {Dept. of Meteorology, University of North Dakota, Grand Forks, ND}

33
34 Correspondence to: J. S. Reid (jeffrey.reid@nrlmry.navy.mil; 1 831-656-4725)
35
36

37 ABSTRACT: In a joint NRL/Manila Observatory mission, as part of the 7 SouthEast Asian
38 Studies program (7SEAS), a two-week, late September 2011 research cruise in the northern
39 Palawan Archipelago was undertaken to observe the nature of southwest monsoonal aerosol
40 particles in the South China Sea/East Sea (SCS/ES) and Sulu Sea region. Previous analyses
41 suggested this region as a receptor for biomass burning from Borneo and Sumatra for boundary
42 layer air entering the monsoonal trough. Anthropogenic pollution and biofuel emissions are also
43 ubiquitous, as is heavy shipping traffic. Here, we provide an overview of the regional
44 environment during the cruise, a time series of key aerosol and meteorological parameters, and
45 their interrelationships. Overall, this cruise provides a narrative of the processes that control
46 regional aerosol loadings and their possible feedbacks with clouds and precipitation. While 2011
47 was a moderate El Nino/Southern Oscillation (ENSO) La Nina year, higher burning activity and
48 lower precipitation was more typical of neutral conditions. The large-scale aerosol environment
49 was modulated by the Madden Julian Oscillation (MJO) and its associated tropical cyclone (TC)
50 activity in a manner consistent with the conceptual analysis performed by Reid *et al.*, (2012).
51 Advancement of the MJO from phase 3 to 6 with accompanying cyclogenesis during the cruise
52 period strengthened flow patterns in the SCS/ES that modulated aerosol lifecycle. TC inflow
53 arms of significant convection sometimes span from Sumatra to Luzon, resulting in very low
54 particle concentrations (minimum condensation nuclei $CN < 150 \text{ cm}^{-3}$, non-sea salt $PM_{2.5} < 1 \mu\text{g m}^{-3}$).
55 However, elevated carbon monoxide levels were occasionally observed suggesting passage of
56 polluted air masses whose aerosol particles had been rained out. Conversely, two drier periods
57 occurred with higher aerosol particle concentrations originating from Borneo and Southern
58 Sumatra ($CN > 3000 \text{ cm}^{-3}$ and non-sea salt $PM_{2.5} 10\text{-}25 \mu\text{g m}^{-3}$). These cases corresponded with
59 two different mechanisms of convection suppression: lower free-tropospheric dry-air intrusion
60 from the Indian Ocean, and large-scale TC-induced subsidence. Veering vertical wind shear also
61 resulted in aerosol transport into this region being mainly in the marine boundary layer (MBL),
62 although lower free troposphere transport was possible on the western sides of Sumatra and
63 Borneo. At the hourly time scale, particle concentrations were observed to be modulated by
64 integer factors through convection and associated cold pools. Geostationary satellite observations
65 suggest that convection often takes the form of squall lines, which are bowed up to 500 km
66 across the monsoonal flow and 50 km wide. These squall lines, initiated by cold pools from large
67 thunderstorms and likely sustained by a veering vertical wind shear and aforementioned mid
68 troposphere dry layers, propagated over 1500 km across the entirety of the SCS/ES-effectively
69 cutting large swaths of MBL aerosol particles out of the region. Our conclusion is that while
70 large-scale flow patterns are very important in modulating convection and hence allowing long
71 range transport of smoke and pollution, more short-lived phenomena can modulate cloud
72 condensation nuclei (CCN) concentrations in the region, resulting in pockets of clean and
73 polluted MBL air. This will no doubt complicate large scale comparisons of aerosol-cloud
74 interaction.

75

76

77 1.0 INTRODUCTION

78 Given its hypothesized sensitivity to global climate change (e.g., IPCC 2007; *Yusuf and*
79 *Francisco* 2009), Southeast Asia (SEA) has experienced a substantial increase in scientific
80 interest; from the region's highly complex meteorology, to its atmospheric chemistry, air quality,
81 and climate. The region, including the Maritime Continent, South China Sea/East Sea (SCS/ES),
82 and Sulu Sea, is thought to be highly susceptible to aerosol cloud interactions (*Rosenfeld*, 1999;
83 *Hamid et al.*, 2001; *Yuan et al.*, 2011). Indeed, around the second half of the boreal summer
84 monsoonal period from August to mid-October, the seasonal dry climate allows biomass burning
85 throughout the Maritime Continent (MC), particularly in warm El Nino-Southern Oscillation
86 phases (e.g. *Nichol* 1998; *van der Werf et al.*, 2004; *Field and Shen* 2008; *Langner and Siegert*
87 2009; *Field et al.*, 2009; *van der Kaars et al.*, 2010; *Reid et al.*, 2012; 2013). Climatologically,
88 there exists both anecdotal evidence and some station data suggesting an increase in the number
89 of no-rain days in the Philippines (*Cruz et al.*, 2013), yet perhaps an increase in intense events
90 (*Cinco et al.*, 2014). Perhaps such a behavior is a result of the effect of increasing aerosol
91 emissions on clouds. At the same time there is a long-standing hypothesis that there are increases
92 in mid-level cloudiness, also perhaps due to increased levels of aerosol particles (*Parungo et al.*, 1994).

93

94 Under most circumstances, smoke and pollution from the MC is thought to be transported by
95 southwesterly monsoonal winds into the SCS/ES where it is scavenged by convection with
96 eventual annihilation in the monsoonal trough (*Reid et al.*, 2012; *Xian et al.*, 2013). However, the
97 transition process between “polluted land” and “clean monsoonal trough” is poorly understood.
98 Large scale modeling studies suggesting smooth transport are at odds with visible imagery (*Reid*
99 *et al.*, 2013) and lidar observations (e.g., *Campbell et al.*, 2013), which suggest smoke is often
100 sequestered on or very near the major land masses. Owing to near ubiquitous high cloud cover in
101 the SCS/ES, there are relatively few satellite observations of smoke transport in the region,
102 except during anomalously clear or severe events. The limited remote sensing data that are
103 available is largely qualitative, with both cloud and aerosol retrievals showing great regional
104 diversity across product lines in this near-ubiquitous cloud environment (*Reid et al.*, 2013).
105 While higher-frequency meteorological phenomena, such as the Madden Julian Oscillation and
106 equatorial waves (*Reid et al.*, 2012), as well as orographic and sea breeze effects, are thought to
107 exert significant influence on transport (*Mahmud*, 2009a,b; *Reid et al.*, 2012; *Wang et al.*, 2013;

108 *Xian et al.*, 2013), there are virtually no in situ observations of the SCS/ES aerosol environment
109 in this critical summer monsoonal season. Cloud processes in regions such as the MC are
110 expected to be sensitive to the presence of aerosol particles (e.g., *Sorooshion et al.*, 2009; *Yuan et*
111 *al.*, 2011; *Lee et al.*, 2012). But, we have little information on how well models perform.

112
113 As part of the 7 Southeast Asian Studies (7SEAS) program (*Reid et al.*, 2013), a two-week
114 research cruise was conducted from September 17- 30, 2011 in the northern half of the Palawan
115 Archipelago of the Philippines; a region thought to be a long range receptor for MC biomass
116 burning and industrial emissions (*Reid et al.*, 2012; *Xian et al.*, 2013). At the same time,
117 additional sun photometer, lidar and ground measurements were made in Singapore to contrast
118 with the Philippine receptor. Other sun photometers were located across Southeast Asia.
119 Conducted on the M/Y *Vasco*, a locally owned 35 m vessel, our goals were to make first-ever (to
120 our knowledge) measurements of near-surface aerosol properties in the region, test the transport
121 hypotheses put forth in *Reid et al.* (2012), and develop new hypotheses on aerosol-weather
122 interaction that regulate aerosol prevalence to be studied in future deployments. *Most*
123 *importantly, we aim to develop a narrative on how model simulations and remote sensing*
124 *retrievals correspond with real world observations in this highly complex aerosol and*
125 *meteorological environment.* Often, the intricacies of aerosol-meteorological relationships are
126 blurred in bulk analyses to the detriment of understanding regional physics and chemistry. Only
127 through studies, such as presented here, can we hope to derive the true sensitivity of the region to
128 aerosol emissions.

129
130 In this paper, we give a brief overview of the cruise and its measurements, as well as other
131 regional measurements made to aid in interpreting the regional aerosol environment. This will
132 form a descriptive basis for subsequent 7SEAS papers on aerosol and cloud features for the 2011
133 burning season, as well as a contrast to a similar 2012 cruise to be reported at a later date. The
134 analysis portion of this paper is focused on the temporal variability of aerosol particle number
135 and mass concentrations and how these relate to regional meteorological phenomenon, such as
136 large scale monsoonal flow, the MJO, TC development and propagation, and large scale squall
137 lines/cold pools. We end with a discussion of the strong covariance between aerosol prevalence
138 and regional thermodynamic behavior, noting how it must be considered in studies of aerosol,

139 cloud, and precipitation interaction.

140

141 2.0 CRUISE DESCRIPTION AND INSTRUMENTATION

142 This research cruise was conducted on the 35 meter, 186 ton M/Y *Vasco*, owned and operated by
143 Cosmix Underwater Research Ltd. Manila, Philippines. Photos of the vessel along with its cruise
144 track are provided in Figure 1. The *Vasco* departed on Sept. 17, 2011 from Navotas, Manila Bay,
145 and returned midday Sept. 30. The target area for the bulk of the monitoring was in the vicinity
146 of El Nido and outside of Malampaya Sound, Palawan Island (Lat=111.1N; Long=119.3E). The
147 general mode of operation was to travel to selected areas, then choose locations for sampling
148 which had a clear breeze to the open ocean, though protected from the sometimes large swell
149 with no local wave breaking. Great care was taken to not position the ship downwind of any
150 sources. Indeed, small settlements are ubiquitous on small islands. But these were all avoided.
151 The ship would move every one to two days within each area to support other physical
152 oceanographic measurements. The route south from Manila included a one-day stop at Apo Reef
153 on Sept. 18, and the coast of Culion on September 19. From Sept. 20 through the morning of
154 September 28th the *Vasco* operated in the northern Palawan area. On the morning of Sept. 29th,
155 the *Vasco* departed El Nido for return to Manila on the early afternoon of Sept. 30th.

156

157 Instrumentation was generally deployed in two configuration groups. Self-contained
158 instrumentation, including meteorology and aerosol chemistry, was located on a 3 m flux tower
159 on the bow of the ship; a total top-to-bottom height of 6 m above the ocean surface. This ensured
160 no self-contamination from the ship except for very rare periods of a following wind. Aerosol
161 particle counters and nephelometers were located in a forward locker fed by a 4 cm diameter/4 m
162 long inlet from the top of the ship. Wind directional data ensured only periods with air moving
163 over the bow were used (to remove periods of contamination and self-sampling from the
164 dataset). Periods of self-sampling were also abundantly clear from CN counts. Such periods were
165 obvious-with rapid particle count fluctuations in the 1000 to 10,000+.

166

167 2.1 Meteorology

168 The meteorological instrumentation set was associated with the 3 m flux tower. While fluxes are
169 a subject of a separate paper, a brief summary is appropriate here. A Campbell sonic anemometer

170 and Licor IR H₂O/CO₂ system were sampled at 50 hz to provide fluxes of momentum, sensible
171 and latent heat. Mean meteorology was also provided by an RM Young propeller anemometer
172 and a Campbell pressure and ventilated temperature and humidity probe. Sea surface temperature
173 was provided by a waterline floating thermocouple. Downwelling shortwave radiation was
174 measured with a Kipp and Zonan CMP 22 radiometer. Ship location and attitude were given by a
175 Garmin GPS and accelerometer package. This attitude and velocity data was used to correct
176 meteorology and solar radiation data.

177
178 In addition to the flux tower, ceiling and visibility were provided by a Vaisala C31 ceilometer,
179 which has been shown to provide information on aerosol particle profiles when properly
180 corrected (e.g., *Clarke et al.*, 2003; *Markowicz et al.*, 2008; *Tsaknakis et al.*, 2011). Twenty-five
181 InterMet 1-AB radiosondes were also released during the cruise, generally one to two per day;
182 twenty of these passed our quality control. Forward-looking automatic cameras logged images
183 every minute.

184 185 2.2 Aerosol and Gas Chemistry

186 A series of aerosol samplers were mounted on the bow of the ship. One of the primary
187 instruments utilized in this paper was a free-standing eight-stage Davis Rotating-drum Uniform
188 size-cut Monitor (DRUM) sampler. The instrument used in this study was a version of the
189 DRUM sampler originally described by *Cahill et al.* (1985), modified to utilize slit orifices and
190 configured to run at 16 L min⁻¹ as described in *Reid et al.* (2008). A similar instrument was
191 deployed for comparison to Dongsha Island in the SCS/ES in 2011 in the winter/ spring
192 Northeasterly Monsoon (*Atwood et al.*, 2013a). An unheated PM₁₀ sample inlet was used
193 upstream of the impactor, followed by collection stages with nominal 50% aerodynamic
194 diameter-cut sizes of 5 μm, 2.5 μm, 1.15 μm, 0.75 μm, 0.56 μm, 0.34 μm, 0.26 μm, and 0.07
195 μm. Aerosol particles were collected on Mylar strips coated with Apiezon grease and wrapped
196 around each rotating drum. The drums were rotated at a consistent rate such that nominal
197 timestamps could be assigned to specific locations along the strip during compositional analyses,
198 yielding 90 minute time resolution. DRUM samples were subjected to X-Ray Fluorescence
199 (XRF) analysis at the Advanced Light Source (ALS) of Lawrence Berkeley National Laboratory
200 to provide measurements of selected elements having atomic weights between Mg and Mo, along

201 with Pb. Unlike previous DRUM analyses described in the literature, the XRF Analysis samples
202 for this study utilized a more advanced detector system, making XRF derivations of key sea salt
203 elements, such as Na and Cl much more quantitative. For simplicity here, time series of
204 elemental concentration data for the eight raw size fractions were combined into two lumped size
205 fractions: Coarse (stages 1-3 or 10-1.15 μm in aerodynamic size), and fine (stages 4-8, or 1.15-
206 0.07 μm), respectively. A more detailed analysis will be provided by a forthcoming paper by
207 *Lagrosas et al. (2014 – manuscript in preparation)*.

208
209 $\text{PM}_{2.5}$ filters were also collected in daily 5 lpm Minivol Tactical Air Samplers (TAS) and
210 analyzed by gravimetric, XRF and ion chromatography at the Desert Research Institute. A
211 second set of filters provided organic and black carbon, by the method of Chow et al. (1993).
212 Finally, PM_{10} and 2.5 samples were collected by the Manila Observatory using both TAS and a
213 three-stage Dylec impactor for gravimetric and ion chromatography analysis. These, too, are
214 discussed in *Lagrosas et al. (2015 – manuscript in preparation)*.

215
216 For trace-gas analysis, forty-six whole air gas samples were collected in electro-polished
217 stainless steel cans for analysis by gas chromatography by the University of California Irvine.
218 See Colman et al. (2001) for details, a full list of 60+ compounds, and relative uncertainties.
219 However, only a few species are presented here (e.g., CO, and few halo and hydrocarbons).
220 Flame ionization detectors (FIDs) were used to measure C_2 - C_{10} hydrocarbons, electron capture
221 detectors (ECDs) were used for C_1 - C_2 halocarbons and C_1 - C_5 alkyl nitrates, and quadrupole mass
222 spectrometer detectors (MSD) were used for unambiguous compound identification and selected
223 ion monitoring. Cans were supplied for the cruise under vacuum, and upon valve release at the
224 ship's bow under headwind, each collected its volume over the course of ~ 20 seconds.
225 Measurement precision varied by species, but was better than 5% for the vast majority of
226 species. The most uncertain was dibromochloromethane at 8%. Cans were opened sporadically
227 throughout the cruise, with at least two samples a day being collected generally in the morning
228 and afternoon. Sampling was generally not performed during rain showers. Additional cans were
229 sampled during excellent or interesting sampling conditions, with the highest frequency during
230 the last few days when the ship was a receptor for smoke. Of the forty-six can samples, five did
231 not pass quality assurance as they had anomalously high hydrocarbon and solvent levels. Given

232 the collection procedure, based over the side on the windward bow of the ship, we are not
233 entirely sure how the contamination may have happened, but suspect it may reflect some local
234 contaminant from the scattered islands in the region. For the purposes of this paper on large scale
235 flow, they are excluded here.

236

237

238 2.3 Ship Aerosol Microphysics and Optics

239 Onboard the *Vasco* were a particle counter, sizers, and a nephelometer. Total particle
240 concentrations were measured by a TSI Water Condensation Nuclei Counter (CPC). Fine and
241 coarse-mode particle size was provided by a DMT bench top Passive Cavity Aerosol Sizing
242 Spectrometer (PCASP), and a TSI Aerodynamic Particle Sizer which were calibrated before and
243 after the cruise. These low-flow rate instruments were behind a dry-rite drying column, which
244 dropped relative humidity to ~50%. However, while the CPC and APS operated without incident,
245 the PCASP suffered a relay failure after the first night at sea (night of Sept 17). This was repaired
246 by Sept 24th for the second half of the cruise.

247

248 For light scattering, we used a TSI three-wavelength nephelometer ($\lambda=445, 550, 700$ nm) at
249 ambient RH, and corrected for truncation/non-lambertian light source errors using Anderson et
250 al. (1996). A three-wavelength Particle Soot Absorption Photometer (PSAP) sampled from the
251 nephelometer stream, and was corrected via *Bond et al.* (1999). A Radiance Research single
252 wavelength nephelometer ($\lambda=532$) was also placed downstream of the drying column. Finally, a
253 Microtops hand-held sun photometer was brought on board as part of the Maritime Aerosol
254 Network (MAN; Smirnov et al., 2011) for measuring Aerosol Optical Thickness (AOT).
255 However, cloudy skies prohibited measurements prior to the last two days of the cruise (Sept 29
256 and 30). Comprehensive studies of aerosol optical properties and size are a subject of a
257 subsequent paper. However, here we use the CPC and PCASP to show time series of basic fine-
258 mode particle number and size properties.

259

260 2.4 Regional AERONET Measurements.

261 In addition to the *Vasco* cruise, a number of other instruments were placed in the region to help
262 monitor the aerosol environment. Most notable, in reference to this paper, was a set of four

263 AERONET sun photometers (*Holben et al., 1998*), located on the map in Figure 2b. Two sites
264 including the Singapore 7SEAS super site (e.g., *Atwood et al., 2013b*), Kuching, Sarawat Borneo
265 (*Salinas et al., 2013*) and Marbel University, Mindanao, Philippines were set up for 7SEAS.
266 Songkhla, Thailand was pre-existing operational. For the purposes of this paper, we focus one
267 parameter, 500 nm daily averaged fine-mode AOT. This was generated from the Level 2.0
268 Spectral Deconvolution Algorithm (SDA) Version 4.1, used to separate fine and coarse-mode
269 contributions to AOT (*O'Neill et al., 2003*). By using the SDA, we can effectively remove thin
270 cirrus contamination (*Chew et al., 2011*) and focus on fine-mode particles from industrial and
271 biomass burning sources.

272

273 2.5 Ancillary Satellite and Model Data

274 Baseline meteorology data are provided by the Navy Global Atmospheric Prediction System
275 (NOGAPS; *Hogan and Rosmond, 1991*). We compared NOGAPS fields to NCAR reanalysis
276 fields (*Kalnay et al., 1996*) for the individual events discussed in this paper and, as we found no
277 substantive differences. NOGAPS data are subsequently used for initializing the offline Navy
278 Aerosol Analysis and Prediction System (NAAPS). NAAPS, the Navy's operational aerosol
279 model, is a global operational $1^\circ \times 1^\circ$ aerosol transport model supporting various operations and
280 research, including the monitoring of biomass burning plumes (*Reid et al., 2009*). NAAPS has
281 been extensively exercised for the Maritime Continent region (e.g., *Hyer and Chew, 2010; Reid*
282 *et al., 2012; Xian et al., 2013*). The emissions, transport, and sinks of a combined pollution
283 product (particulate organic matter plus sulfates), open biomass burning smoke, and dust are
284 simulated, and quality-assured AOT retrievals from MODIS observations are assimilated into the
285 model (*Zhang et al., 2008*). Model output includes predicted speciated mass concentrations and
286 AOT. The NAAPS data were used to provide a regional assessment, as well as along the ship
287 track.

288

289 To establish mid and upper-troposphere air-mass source regions, and the large scale flow pattern
290 for selected periods of the cruise, back trajectories were generated using the NOAA Hybrid
291 Single Particle Lagrangian Integrated Trajectory (HYSPLIT) Version 4.9 Model (*Draxler &*
292 *Hess, 1997, 1998; Draxler, 2004*). The GDAS1, $1^\circ \times 1^\circ$ global meteorological dataset, generated
293 for HYSPLIT from the Global Data Assimilation System model, was used to run 72 hr

294 backwards trajectories.

295

296 Numerous satellite products (visible, IR, cloud heights, scatterometer, etc.) are also used in an
297 imaging capacity to aid in the analyses. These can all be found on the NEXSAT system (*Miller et*
298 *al.*, 2006; <http://www.nrlmry.navy.mil/nexsat-bin/nexsat.cgi>) and are cited as used in this paper.

299 We also use other retrieved products for context, such as the Climate Prediction Center (CPC)
300 MORPHing technique (CMORPH, *Joyce et al.*, 2004) for precipitation and derived data
301 assimilation-grade satellite AOT products from MODIS (*Zhang et al.*, 2008) and MISR (*Kahn et*
302 *al.*, 2009). MODIS fire counts are also used here, following the regional interpretation of Hyer et
303 al. (2013). While it would have been highly valuable, CALIPSO data were not collected during
304 the cruise period due to solar anomalies. However, we do present a single collect from Oct. 1 in
305 conditions we believe to be representative of the last few days of the cruise.

306

307 3.0 RESULTS I: REGIONAL METEOROLOGICAL AND AEROSOL CHARACTERISTICS

308 The *Vasco* cruise occurred in the second half of the month of September, 2011. This period is
309 typically towards the end of the boreal summer southwest monsoon (henceforth SWM) system,
310 approximately two to three weeks before the transition period to boreal winter/spring northeast
311 monsoon (NEM). A general overview of the summer monsoonal system can be found in *Chang*
312 *et al.* (2005), *Moron et al.* (2009) and the book by *Chang et al.* (2011). An overview of how
313 monsoonal weather features relate to smoke emissions and transport from progressively larger to
314 finer scales can be found in *Reid et al.*, (2012); *Xian et al.*, (2013), *Mahmud* (2009a,b) and *Wang*
315 *et al.*, (2013), respectively. A brief description of key meteorological and aerosol elements for the
316 summer 2011 burning season, as they relate to the study measurement period, is provided here.

317 3.1 Overall Nature of the Meteorological and Aerosol Environment.

318 As discussed in the references above, the SWM in the greater Southeast Asian region is generally
319 between mid-April and mid-October. Associated lower-atmospheric flows in the MC are easterly
320 when south of 3°S, and westerly when north of this latitude. In the SCS/ES, surface winds turn
321 southwesterly, eventually terminating in a monsoonal trough east of the Philippines. In the upper
322 free troposphere over the SCS/ES, winds flow in the opposite direction to the marine boundary
323 layer and lower free troposphere: generally north-easterly, originating from the monsoonal

324 trough. The ~500 hPa level generally is the delineation between southwest winds below and
325 northeast winds above. Winds at these mid-levels are generally light.

326 For the purposes of this paper, the general meteorology during the cruise is depicted in Figure
327 2(a), where NOGAPS surface and 850 hPa winds (black & magenta, respectively) are provided.
328 These two levels bound the vast majority of aerosol particles in the region during the SWM
329 (*Tosca et al.*, 2011; *Campbell et al.* 2013; *Chew et al.*, 2013; *Wang et al.*, 2013). Average study
330 period precipitation from CMORPH is also provided as the color background. The red star in the
331 northern Palawan area indicates the *Vasco's* position during the bulk of the sampling. Figure 2(b)
332 provides a map of all MODIS (Terra+Aqua) fire counts during the study period. Here, green stars
333 indicate relevant AERONET sun photometer data utilized in this study. Finally, Figure 2(c)
334 provides the average MODIS + MISR AOTs for the mission, although readers should be aware
335 that AOTs in the northern half of the domain were derived from only the last few days of the
336 study when skies were clear enough to perform a retrieval (this is discussed in more detail later).

337 The wind fields in the SCS/ES during the study period were largely typical for the SWM season,
338 with its prevailing southwesterly winds, averaging ~8-20 m s⁻¹ over most of the region. The
339 transition from easterlies and southeasterlies south of the equator to southwesterlies in the
340 SCS/ES can be seen in the general wrapping of the winds around Borneo and Sumatra. Wind
341 strength anomalies were generally low over the region, although in the middle of the SCS/ES
342 positive anomalies were on the order of 7 m s⁻¹. Clear cyclonic activity in the northern SCS/ES
343 region is also apparent. As we discuss later, these positive wind anomalies are result of TC
344 activity and inflow arm wind enhancement during the cruise. Also notable is the slight veering
345 wind shear at lowest levels. While the surface winds are clearly southwesterly, they do become
346 more westerly through the lower free troposphere to 700 hPa. As discussed later, this has
347 significant implications for regional aerosol transport and convection.

348 Precipitation is a maximum along the monsoonal trough, which extends from the northern
349 SCS/ES to the southeast. However, during the mission, precipitation was not continuous in this
350 region, but was rather a composite of enhanced local precipitation, lows, squall lines and tropical
351 cyclone development. Secondary precipitation maxima were visible and include 1) convection
352 over land; 2) precipitation west of Sumatra in the so called West Sumatran Low, and 3)
353 convection east of Myanmar driven by convergence of oceanic air masses reaching land. A

354 depiction of the diversity of regional cloud features during the mission can be seen in Fig. 3. An
355 area of near absence of precipitation south of southern Borneo and southern Sumatra except for
356 isolated mountain top convection, encompassing such islands as Java and Timor, is a common
357 feature of the SWM.

358 The 2011 season corresponded to a moderate La Nina year (Multivariate ENSO Index= -0.95).
359 This typically implies higher precipitation and less fire activity than normal (*Field and Shen*
360 *2008; Field et al., 2009; Reid et al., 2012*). However, in this particular year, precipitation and fire
361 activity were more characteristic of a neutral year. Thus, while fire activity and smoke AOTs
362 were not akin to the boreal summer El Nino events of 1997, 2004, 2006 and 2009, 2011 ranks in
363 the middle third in our estimate of fire activity since 2000 (based on *Reid et al., 2012* statistics).
364 As is typical for the late SWM, fire activity was concentrated in southern Sumatra and southern
365 Borneo/Kalimantan. Fires in this region are often associated with peatland burning, although a
366 great deal of plantation and small holder slash burning is common (See *Reid et al., 2013* for a
367 discussion of regional burning practices). As actual peat burning is much more common in
368 drought years (e.g., *Field and Shen, 2008; Miettinen et al., 2010; 2011*), we suspect much of the
369 observed burning was associated with agricultural maintenance or deforestation.

370 Intermediate fire activity corresponded with moderate AOT in the region, as can be seen in Fig.
371 2(c) that provides average composites of MISR and MODIS (Terra+Aqua) AOT. Near the
372 biomass burning sources, AOTs can be high, averaging over 1 for $\lambda=550$ nm. This is likely low-
373 biased, as AOT retrievals often flag thick aerosol plumes as cloud in the region (*Reid et al.,*
374 *2013*). Comparison of the Figure 2 panels elucidates regional transport patterns: smoke generated
375 in Sumatra and Borneo is carried by the southwesterly winds through the SCS/ES and eventually
376 scavenged out. Some Sumatran smoke also crosses the island's western mountain range and
377 enters the Indian Ocean. While model representation of regional smoke transport often suggests a
378 smooth transition, imagery, and both passive satellite and lidar observations, often depict a strong
379 gradient between island and ocean (e.g., *Campbell et al., 2013; Reid et al., 2012, 2013*).
380 Prevailing hypotheses for this divergence surround scale-dependent issues in the model, and the
381 reproducibility of orographic and sea breeze meteorology (e.g., *Reid et al., 2012; Wang et al.,*
382 *2013; Xian et al., 2013*). But overall, the transport and transformation mechanisms from polluted

383 island to clean marine background air are not well understood nor easily simulated. This paper,
384 as well as subsequent efforts based on this cruise, hope to address these problems.

385 *3.2 Evolution of the meteorological environment during the Vasco cruise*

386 The timing of the *Vasco* cruise was serendipitous, as it coincided with the transition of the MJO
387 from wetter to a drier phase in the MC. The MJO is a large-scale, coupled pattern of meso-
388 synoptic scale circulation and deep convection that forms in the Indian Ocean and propagates
389 eastward at $\sim 5 \text{ m s}^{-1}$ through and around the MC and into the Pacific Ocean (*Madden and Julian,*
390 *1971; Zhang, 2005, 2014*). Phase and amplitude of the MJO are quantified for this study using
391 the method of *Wheeler and Hendson (2004)*. Once this convective region passes into the
392 central/eastern Pacific and decays, a new event may start in the Indian Ocean, repeating the
393 cycle. From an aerosol point of view, while ENSO is an excellent large-scale indicator of
394 seasonal burning, the wet and dry phases of the MJO strongly influence the intraseasonal timing
395 of significant smoke events in the MC (*Reid et al., 2012*). While the MJO was hypothesized to
396 influence overall AOT (*Tian et al., 2008*), no satellite-based AOT verification of this has yet been
397 established due to the difficulty in performing aerosol remote sensing in the region (*Reid et al.,*
398 *2013*). However, fire observations are strongly enhanced in dry phases (*Reid et al., 2012*) and
399 mechanistically a relationship between dry MJO phase, fire emissions, and high AOT seems
400 certain.

401
402 An important correlation of MJO-related convection as it transits and departs the MC is an
403 associated increase in the formation of regional TCs (*Maloney and Hartman, 2001*). *Reid et al.,*
404 *(2012)* noted that when TCs transit the SCS/ES there is an increase in both fire activity in the
405 southern MC and ventilation of smoke into the SCS/ES region. This relationship is thought to be
406 associated with an acceleration of southwesterly winds in the SCS/ES as air approaches the TC.
407 As TCs enter the area, strong convection develops along the inflow arm, scavenging smoke
408 transported offshore. Later, as the TC passes, large-scale subsidence follows, resulting in
409 negative precipitation anomalies over much of the SCS/ES and MC. An example of such a case
410 is presented in global and mesoscale simulations in *Reid et al. (2012)* and *Wang et al. (2013)*,
411 respectively. Over the period of Sept 17-30, the MJO convective active phase migrated out of the
412 MC (that is migrated from Phase 3 to Phase 6) at a relative strength that increased above the one

413 standard deviation intensity level halfway through the period. The migration of the MJO
414 coincided with a train of TC activity beginning Sept 23.

415 Select examples of daily mean winds with precipitation and representative daytime MTSAT
416 visible images are found in Figures 3(a)&(b), respectively. On Sept 17, the day of departure, the
417 general meteorology of the SCS/ES and MC was fairly typical for a convectively-active phase of
418 the MJO. Regional lower-tropospheric winds exhibited small anomalies against the NCEP
419 climatology. Comparison of the CMORPH-derived precipitation (Figure 3(a)) with MTSAT
420 visible images (Figure 3(b)) suggested the whole region was showery, with light scattered
421 precipitation from many small to medium-sized cells and a few deep and intense storms. Some
422 organization can be seen, however, in an 800 km wide area in the SCS/ES between southern
423 Vietnam and Borneo. Over the next forty-eight hours (Sep 19), precipitation over the region
424 increased, and the patch of convection in the SCS further organized and intensified. By Sept 22,
425 convection intensified further over the whole SCS/ES, and cyclonic rotation became clearly
426 evident around a tropical depression in the northern SCS. This coupled system resulted in lines
427 of convection and heavier precipitation from the southwest to the northeastern side of the
428 SCS/ES. The tropical depression was later named Tropical Storm 21 W- Haitang. Haitang
429 continued developing until Sep 25th, reaching maximum winds of 18 m s⁻¹. The inflow arm of
430 Haitang moved westward, leaving the southern SCS/ES drier.

431 As Haitang was beginning to develop, a separate system, 20 W Nesat, rapidly intensified in the
432 western Pacific Ocean and migrated westward. As Haitang then migrated into northern Vietnam,
433 Nesat developed, making landfall on Luzon on Sep 26 with maximum one-minute sustained
434 wind speeds of ~58 m s⁻¹ –ultimately listed as a Category 4 TC. After passing Luzon and causing
435 an estimated \$1B damage, Nesat lost strength to Category 1 before making landfall again at
436 Hunan Island on September 29. Finally, the third tropical cyclone, the westward-tracking
437 Typhoon #22W Nalgae made landfall in northern Luzon as a more compact but stronger
438 Category 4 storm (67 m s⁻¹ sustained) on October 1. Detailed discussion of these storms can be
439 found in the Joint Typhoon Warning Center Annual Tropical Cyclone Report
440 (<http://www.usno.navy.mil/NOOC/nmfc-ph/RSS/jtwc/atcr/2011atcr.pdf>)

441 These three tropical storms changed the nature of the regional meteorology for the second half of
442 the cruise, and as we discuss, modulated regional aerosol loadings. Satellite imagery clearly

443 showed the region oscillating between significant convection, developing in inflow arms (e.g.,
444 Sept. 22 & 27) across the SCS/ES, followed by areas of considerable clearing (e.g., Sept 24-25 &
445 29-30). Inflow arms corresponded with increases in southwesterly winds, perhaps further
446 ventilating MC air into the SCS/ES region.

447

448 *3.3 Evolution of the overall aerosol environment during the Vasco cruise period*

449 To provide context to regional fire and aerosol behavior during the *Vasco* cruise, time series of
450 fire activity and AOTs are given in Figure 4. Figure 4(a) shows the MODIS fire hotspot time
451 series for key regions in the MC for the 2012 burning season. As explained in *Reid et al. (2012)*
452 to account for satellite orbit, some smoothing of the data are required; in this case a 5 day boxcar
453 is used. Four fire events are visible over the course of the SWM. First, an early-season event in
454 late July/early August is visible in Central Sumatra and Indonesian Kalimantan (predominately
455 western Kalimantan); this is associated with early agricultural burning. A second and much more
456 significant peak in late August is found in Southern Sumatra and Indonesian Kalimantan
457 provinces predominately in the south. This is fairly anomalous behavior, especially for a La Nina
458 year, as this region typically burns very late in the season (*Reid et al., 2012*).

459

460 In September, two more events, one early and one late in the month, are visible. The first,
461 peaking around September 7th is region wide, but is dominated by Sumatra. The last major event,
462 which corresponded with the *Vasco* cruise, peaked September 26th, with major contributions
463 from southern Sumatra and Kalimantan and more minor contributions from islands to the south
464 of Borneo. As noted in *Reid et al. (2012)*, these peaks in observed fire activity often correspond
465 to dry MJO phases (e.g., Aug. 23, Sept. 26) or overall weak MJO activity (e.g., Sept. 5). The
466 period of July 20- August 8 corresponded with a late-phase MJO event. A new MJO event
467 formed August 18. We suspect drying ahead of the convective portion of the event perhaps
468 allowed southern Kalimantan to burn more readily on August 23rd. The wettest phase of the MJO
469 (phase 3) was in the MC from Aug 28-Sept 18. A break in precipitation in the southern MC
470 allowed the Sept 8th fire event, which was dominated by southern Sumatra, and the border of
471 more significant precipitation to the north. It is emphasized, however, that while we believe plots
472 such as Figure 4(a) are indicative of qualitative fire patterns, they are nevertheless influenced by
473 clear sky bias, which also corresponds with MJO activity.

474

475 While the MC generally has high background aerosol concentrations from pervasive industrial,
476 shipping and biofuel sources (*Reid et al.*, 2013), peaks in AOTs from AERONET sites largely
477 match fire activity. Fine-mode AOT from four sites are shown in Figure 4: (b) Singapore; (c)
478 Songkhla (further up the Malay Peninsula in peninsular Thailand), (d) Kuching in Sarawak
479 Malaysia, Borneo, and e) Notre Dame of Marbel University on Mindanao. Fine mode AOTs
480 from sites near sources typically ranged from 0.1-0.3 during background conditions, and 0.4-1.0
481 during biomass burning events. For the most part, the August 23rd event was the largest region
482 wide, with significant spikes in both Singapore (impacted from Sumatra) and Kuching (impacted
483 largely by southern Kalimantan). The September 7th event is also visible in Singapore, but there
484 is little indication of smoke over Kuching. The *Vasco* cruise period captured the last AERONET
485 AOT peaks for the season in Singapore, Kuching and in particular Mindanao. This establishes
486 that the ship was well positioned as a long range receptor for transport from the MC into the SW
487 monsoonal trough.

488 Because of the generally small fraction of clear sky, frequent high thin clouds, and sometimes
489 extreme AOTs in the region, it is difficult to apply satellite AOT retrievals in a straightforward
490 manner. In particular, sampling bias can be pervasive (*Zhang and Reid*, 2009). However, the
491 AOT analyses in Figure 4 that are associated with the meteorological modes presented in Section
492 3.2 are illustrative of regional aerosol loadings: (f) MJO Active phase: Sept 17-22; (g) MJO
493 transition and TC active phase: Sept 23-27; and (h) post TC environment and clearing: Sept 28-
494 30. These AOT maps, coupled with the large-scale flow patterns shown in Figure 2&3, are
495 suggestive of a large-scale southwesterly transport event from the MC to the SCS/ES region in
496 the latter half of the cruise. Early in the cruise, while burning was at a minimum, moderate AOTs
497 still existed in the vicinity of Sumatra and Borneo. Air was relatively clean north of the equator.
498 During the development of the TC active phase, the accelerated burning resulted in a two-to-
499 three factor increase in observed AOTs in the source regions. Smoke being transported into the
500 SCS/ES, Celebes Sea, and Sulu Sea is clearly visible. Due to clearing in the post TC phase,
501 retrievals were then possible over much of the region. Heavy smoke is observed as far as 10° N,
502 with moderate AOTs extending past Luzon. Cleaner air masses with AOT<0.125 are clearly
503 visible on the western side of the Philippines. Thus, from the time series in both Figs. 2 and 4, we
504 would expect aerosol concentrations to increase as air masses entered the convective regions of

505 the SCS/ES. As no satellite retrievals were ever made on the track of the *Vasco*, a question
506 remains as to the aerosol concentrations within the active regions. This is addressed in the next
507 section where we discuss environmental time series from the *Vasco*.

508 From an aerosol modeling perspective, Figure 5 presents a time series of AOT, surface
509 anthropogenic fine-mode concentrations, and biomass burning provided by the NAAPS
510 reanalysis for key transitional days. Through use of AOT data assimilation and satellite
511 precipitation to constrain wet deposition, this is a reliable global model scale perspective of
512 aerosol transport in this data sparse region. Shown are four of the days in Figure 3: Sep 18, 22,
513 24, and 30. By and large, modeled aerosol fields match our expectations from the meteorology.
514 While AOTs are high near source areas in the first half of the cruise, convection over the SCS/ES
515 quickly scavenged aerosol particles near shore. This was particularly true for periods with well-
516 established TC inflow arms. In the second half of the cruise, two strong injection and transport
517 events carried aerosol particles as far north as Luzon. These events were separated by TC Nesat.
518 The relative strengths of anthropogenic pollution versus biomass burning suggest significant
519 burning enhancement in the last days of the cruise. Of particular note is that in the middle portion
520 of the cruise, model and flow data suggest the northern Palawan region was most dominated by
521 transport up the SCS/ES from the Java Sea and Southeastern Borneo, with the Sulu Sea being
522 dominated by transport from eastern Borneo through the Celebes Sea. This Sulu Sea flow pattern
523 then dominated for the last few days of the cruise, although as discussed in the next section, we
524 suspect some additional industrial sources in the final day.

525 Finally, aerosol vertical distribution is a crucial element of the system. Unfortunately, CALIPSO
526 was placed in standby mode from Sep 22-30 due to solar flare activity. For the early cruise (Sept.
527 17-22) thick regional cirrus cover and orbital track conspired to prevent meaningful aerosol data
528 collections. However, the NAAPS reanalysis does provide a simulation of aerosol vertical
529 distribution, and we checked for consistency once CALIPSO data was made available for Oct. 1st
530 when cirrus optical thickness was low enough to profile the aerosol layers underneath. These
531 data are presented in Figure 6. Meridional cross sections for total fine-mode aerosol particle
532 concentration are provided for Sept. 24 and 30, for 110° and 120°E longitude across the SCS/ES
533 and Sulu Sea regions. These meridians are marked on the AOT plots of Figure 5. At Borneo and
534 immediate outflow regions, NAAPS generally keeps the bulk of the aerosol mass concentration

535 below 3 km, in line with previous remote sensing (*Tosca et al.*, 2011; *Campbell et al.*, 2013) and
536 higher resolution modeling efforts and comparison (*Wang et al.*, 2013). We can interpret this as
537 smoke mixing through a deep planetary boundary layer, including the PBL cloud entrainment
538 zone. This deep layer progresses well offshore east of Borneo in the Celebes Sea. However, as
539 we go further into the SCS/ES and Sulu Sea, fine-mode aerosol particles concentrations are
540 increasingly predominant in the lowest kilometer.

541 CALIOP data in Figure 6, collected on Oct. 1, 2011 (the day after the Vasco returned to port but
542 still probably representative of the second large event), shows the same features, with perhaps an
543 aerosol layer aloft at 1-2 km in North Western Borneo, but a sharp aerosol layer below 1 km
544 across the SCS/ES region. In this case, the scale heights are even lower than NAAPS, perhaps
545 due to numerical diffusion in the vertical in the model. This regional transition from deeper to
546 shallower aerosol scale height, as one moves out in the SCS/ES, is seen very clearly in
547 climatological lidar data (e.g., *Campbell et al.*, 2013). In the context of this cruise, we can
548 explain it as a result of the veering wind shear in the lowest portion of the atmosphere. Aerosol
549 particles in the MBL are transported with a more southwesterly wind. At 850 hPa and above,
550 winds are more westerly. Thus, aerosol particles at higher levels are transported eastward rather
551 than north. Similarly, convective lofting into the lower troposphere will then place the aerosol
552 particles in a westerly wind, and thus any northward component of transport must be associated
553 with the MBL. This finding makes understanding the sea breeze induced ejection of smoke on
554 the western side of Borneo all the more important in the simulation of smoke transport to the
555 Philippines and the monsoonal trough. For eastward transport off of eastern Borneo, the
556 boundary layer and lower free troposphere winds have similar directions. Hence, we find deeper
557 aerosol layers in the Celebes Sea. Based on the climatological aspects of wind shear (e.g., *Reid et*
558 *al.*, 2012), we expect this generally explains the climatological aerosol vertical distribution in the
559 region presented by *Campbell et al.*, (2013). This finding also suggests that the surface sampling
560 by the Vasco was largely indicative of smoke and pollution transport, and is representative.

561 4.0 RESULTS II: VASCO METEOROLOGY AND AEROSOL TIME SERIES

562 As Section 3 has established the overall nature of the lower troposphere, we can begin to
563 interpret the measurement time series from the *Vasco*. In particular, we wish to understand how
564 the large-scale conceptual models and observations presented above relate to real world marine

565 boundary layer meteorology and aerosol phenomena. Key meteorological and aerosol
566 measurements, which best depict the overall environment, are presented in Figure 7. Included are
567 the meteorological parameters: (a) pressure; (b) temperature; (c) wind speed;; and (d)
568 precipitation rate. Key aerosol parameters include (e) the 30-min average water CPC total
569 aerosol concentration; (f) the estimated PM_{2.5} mass concentrations from filters (corrected to
570 remove sea salt by subtracting sea salt based on 3.26* Na concentration) and organic and black
571 carbon from quartz filters. Also shown are grab-can samples of CO; (g) PM₁ ammonium sulfate
572 (NH₄)₂SO₄ in red (based on DRUM sampler S assuming all non-sea salt S was in (NH₄)₂SO₄)
573 with coarse-mode sea salt in blue (1-10 μm, based on the Na*3.26 method), and finally (h)
574 NAAPS-derived total fine-mode particle concentration, differentiated between biomass burning
575 and a combined interactive anthropogenic +biogenic product.

576 Marked on Figure 7 are points of interest during the cruise to be discussed herein. They begin
577 with departure from Manila Harbor, followed by our exit from Manila Bay. Our first point of
578 stationary sampling was at Apo Reef, followed the next day at the West Coron site. Long time-
579 period stationary sampling was then conducted at Guntao Island just outside of El Nido, then just
580 outside Malampaya Sound, and then back at Guntao Island again. During the last Guntao Island
581 measurement period, the *Vasco* experienced the largest cold pool event, a topic of discussion of
582 Section 4.2. Late on Sept 26, the *Vasco* took shelter from Typhoon Nesat in Liminangcong
583 harbor, which showed considerable local contamination. Once there was suitable reduction in
584 significant wave heights, the *Vasco* moved north to just outside El Nido harbor to enable more
585 regional sampling. On the morning of September 29, the *Vasco* had to return to Manila harbor via
586 the Mindoro Strait ahead of TC Nalgae. In preparation for Nalgae, our equipment was shut down
587 and boxed up one third of the way into Manila Bay midday on Sept 30.

588 Based on a preliminary analysis of NAAPS data (e.g., Figure 5), boundary layer air sources were
589 all coastal Borneo or Southern Sumatra/Java Sea for most of the cruise. The two important
590 exceptions were in the first day and last two days of the cruise, when model and trajectories
591 suggest some influence from northern Borneo the Celebes Sea. As discussed above, winds
592 veered with height, with the lower free-tropospheric air tracing an origin to the Malay Peninsula
593 and Indian Ocean, where pollution and biomass burning emissions are significantly reduced.
594 Thus, we expect highest particle concentrations to be in the MBL.

595 4.1 Daily scale meteorological and aerosol concentration features

596 To understand the nature of the coupled meteorological-aerosol environment we have to
597 reconcile large scale meteorological and remote sensing analyses with the data at a single
598 receptor point (i.e., *Vasco*). Clearly from Figure 7, both the meteorology and atmospheric
599 composition observed on the cruise are a convolution of low to high frequency signals. To begin
600 the analysis, we consider features with scale of a day or longer.

601
602 As we would expect for a tropical region, overall we see a large measure of consistency in many
603 meteorological features. At daily scales, pressure is relatively constant for the cruise with the
604 exception of a moderate dip ~Sept 26-29 associated with TC Nesat and an embedded diel-solar-
605 tidal signal. Baseline temperatures are also constant at ~28°C, with a 2°C dip also associated with
606 heavy rains from the TC. Surface winds were generally 5-10 ms⁻¹ and typically from the
607 Southwest with occasional departure to the north. Precipitation was showery throughout, with
608 precipitation visible in some form most days, but with the most significant events in the outer
609 rain bands associated with TC Nesat. Embedded in these daily scale features are clear high-
610 frequency phenomena; for example, inverse ramp drops in temperature, with associated spikes in
611 wind speed, and often precipitation. As discussed in Section 4.2, such high-frequency
612 phenomena are largely associated with convective cells and their associated cold pools.

613
614 Within the cruise, we see several large-scale aerosol features. Certainly, just before the *Vasco* left
615 Manila Harbor and Bay, we observed a high spike in particulate matter, indicative of local
616 pollution. However as the *Vasco* departed, we entered a cleaner greater-bay regime, upwind of
617 Manila Bay sources. Outside of Manila Bay, a spike in particulate matter was also observed,
618 likely due to local Luzon influence such as from Batangas. “Regional” SCS/ES monitoring was
619 initiated with the *Vasco*’s first anchorage at Apo Reef in Mindoro Strait on September 18. A more
620 typical background period was observed through midday Sept. 22nd, followed by a significant
621 aerosol event ~Sept 24rd – 26th ended by the arrival of TC Nesat. A second even larger event then
622 followed from late Sept 28 through the return on Sept 30th.

623
624 From the Apo Reef to the northern Palawan anchorages on September 23rd, the *Vasco* was in a
625 very clean aerosol regime. CN counts were generally on the order of ~300-500 cm⁻³, and non-sea

626 salt $PM_{2.5}$ was $\sim < 2 \mu\text{g m}^{-3}$. PM_{10} sea salt was on the order of $5 \mu\text{g m}^{-3}$. Both fine and coarse
627 particle mass are in line with expectations in a background marine atmosphere (Quinn et al.,
628 1996; Henintzenberg et al., 2000; Reid et al., 2006). On Sept 22nd, particle concentrations
629 reached a mission minimum, with sustained CN concentrations below 150 cm^{-3} , and non-sea salt
630 $PM_{2.5} < 1 \mu\text{g m}^{-3}$; at or below our minimum detectable limits. Coarse-mode sea salt remained
631 relatively constant, increasing slightly to $6 \mu\text{g m}^{-3}$. During this time period, however, we found
632 variable CO grab sample data ranging from 80-118ppbv, uncorrelated with particle properties.
633 This first period can be explained through the development of TC Haitang near the SCS/ES, and
634 the formation of a broad southwest to northeast inflow arm on Sept 22 clearly visible in Figure 3.
635 As the inflow arm developed, winds accelerated and precipitation from both shallow and deep
636 convective cells increased. Thus, while Borneo/Java Sea air was clearly being transported to the
637 *Vasco* receptor, precipitation scavenged most fine particles, leaving insoluble trace gases but few
638 particles. Pulses of slightly-enhanced CO nevertheless reached the ship. NAAPS correctly
639 captures this period as relatively clean, although total mass concentrations are high by $\sim 2\text{-}3 \mu\text{g}$
640 m^{-3} .

641
642 The first observed regional aerosol event having a clear Indonesian or Malay source was initiated
643 on Sept. 23, when Haitang moved westward, leaving clearer skies and lighter winds. The *Vasco*
644 remained at the same anchorage outside of El Nido for this entire event. This period saw a slow
645 development in particle concentrations and CO and was largely precipitation free. Non-sea salt
646 $PM_{2.5}$ was on average $8\text{-}9 \mu\text{g m}^{-3}$, with black carbon and organic carbon mass fractions on the
647 order of 5 and 20%, respectively. Corresponding CN counts were on the order of $1000\text{-}2000 \text{ cm}^{-3}$.
648 This period also corresponded with reduced surface winds across the SCS/ES, and an
649 associated slight reduction in coarse-mode sea salt. A significant dip in particle concentrations
650 and temperature was observed late Sept 24th UTC (~ 3 AM local time), which, as we discuss in
651 Section 4.2, was associated with a strong trans-SCS/ES convection-cold pool event. Finally, fine
652 particle mass concentrations reached a maximum and then fell precipitously with the arrival of
653 storm conditions associated with TC Nesat. NAAPS identified this event well as a mixture of
654 anthropogenic and biomass burning sources, although total fine-mode mass concentration is
655 overrepresented by $\sim 30\%$. We suspect this is a result of a low bias in the NOGAPS RH field,

656 which in the context of AOT data assimilation well upstream of the *Vasco*, results in an
657 overestimation of dry mass relative to ambient scattering.

658
659 During the storm period, the *Vasco* was in safe harbor at Liminangcong; the high and variable
660 CN are due to local harbor emissions. After TC Nesat passed, the *Vasco* returned to El Nido for a
661 day of measurements and eventual departure back to Manila. This cruise return period was
662 associated with very light winds and the highest observed particle concentrations, perhaps with a
663 Borneo source. Again, such fair weather is expected on the back side of a strong tropical cyclone
664 such as Nesat, and was further reinforced with the impending arrival of another Category 4
665 storm, TC Nalgae (Figure 3, Sep 30). Fortunately, the typical southwesterly winds slackened to
666 such an extent that the ships own velocity kept air moving over the bow, thus avoiding self-
667 sampling that would have ruined the return period dataset. A time-series analysis of model and
668 trajectory shows that, leading up to this event, transport associated with the last vestiges of the
669 TC Nesat's influence in accelerating regional winds brought the air mass up to the sampling
670 region. Due to wind shear, it is possible it included contributions from both western and eastern
671 Borneo. While we cannot dismiss the possibility of local contamination in the gas can samples
672 while we were in safe harbor in Liminangko, we do see a steady increase in CO reaching a
673 plateau during the final event.

674
675 As the *Vasco* left El Nido, black and organic carbon mass fractions were on the order of 5% and
676 40% suggestive of biomass burning dominance. This period also afforded the only cirrus-free
677 conditions for Microtops sun photometry measurements. 500 nm AOTs were on the order of
678 0.30, very similar to the MODIS retrievals shown in Figure 4(h). NAAPS also captured this
679 event well, and yielded a correct 0.3 AOT. However, like the previous event, total particle
680 concentrations are biased high. Again, we suspect this is due to a low bias in the NOGAPS RH
681 fields. Even so, NAAPS suggests a significant enhancement in biomass burning particle
682 concentrations relative to anthropogenic pollution.

683
684 Based on back trajectories, NAAPS simulations, and particle concentrations, one would initially
685 be inclined to believe the *Vasco* sampled one air mass on its return to Manila. However,
686 examination of wind data shows westerly to northerly winds at the very end of the mission. This

687 plus chemistry (Section 4.4 and Lagrosas et al., 2015, *manuscript in preparation*) show that in
688 the last six hours of the cruise there are slight perturbations to the sources, perhaps a change in
689 the mixture of biomass burning and industrial pollution or the addition of a regional shipping
690 signal. Indeed, across the horizon on Sept 30 we saw many high polluting vessels with plumes
691 visible from 10-30 km away.

692
693 A final consideration for large scale observations is how aerosol loading covaries with
694 atmospheric soundings, perhaps influencing interpretation of aerosol, cloud and precipitation
695 interaction studies. Figure 8 presents three example cases where we found isolated convection,
696 Sept 18th, 25th, and 29th. Sept 18 was our first stop at Apo Reef, where we observed relatively
697 clean aerosol conditions and isolated convection. Over the twenty-four hour period we observed
698 many warm rain events with significant precipitation, as shown in Figure 8(a) & 7(e). For
699 intermediate pollution on September 25th, we encountered significant amounts of boundary layer
700 clouds, but little precipitation (Figure 8 (b); Figure 7(d)). On the other end of the spectrum, Sept
701 29th was indicative of polluted conditions where there were few boundary layer clouds, but
702 occasional significant convection (Figure 8 (c); Figure 7(d)). Simple correlation studies and
703 current scientific thinking would suggest these cases epitomized aerosol-cloud-precipitation
704 interactions. That is, in clean conditions, we have significant amounts of warm rain. If aerosol
705 particle concentrations are perturbed from background conditions, warm rain ceases, and perhaps
706 there is enhancement in severe cells. However, as demonstrated in Figure 8(d)-(f), atmospheric
707 soundings were very different for these cases. Being the tropics, one expects relatively
708 conditionally-stable potential temperature profiles, which indeed we found to be largely the case
709 (Figure 8(d)). But, we can see that for the polluted Sept 25th case, a clear stronger inversion is
710 present at 700 hPa. This inversion corresponds with a lower free-tropospheric dry layer between
711 900-700 hPa with both halved water vapor mixing ratio (Figure 8(e)) and relative humidity
712 (Figure 8(f)). This certainly impaired the development of warm rain formation, even without
713 possible aerosol effects. For the most significant biomass burning event (Sept 29th), the PBL was
714 drier than was typical, yet the lower troposphere was relatively moist. But in this case, large TC
715 induced subsidence produced a dry layer in the mid to upper troposphere, strongly capping
716 convection.

717 To better understand the nature of dry stable layers, Figure 9(a)&(b) present back trajectories
718 initiated at the key “dry altitudes” of 1.6 km (850 hPa) and 6.8 km (500 hPa), respectively, for
719 our cases of Sept. 18, 25 and 29. Tick marks are located every twenty-four hours, and time-
720 height dependencies are provided. For the lower free troposphere, we see clear differences
721 between Sept. 18th and the 25th & 29th, with the 18th originating from convection off of Borneo.
722 For both the 25th and 29th, the lower-to-middle free tropospheric air originated in the Indian
723 Ocean. The NOGAPS time-height cross section over the Phuket, Thailand radiosonde site clearly
724 shows a dry air intrusion into the region between 2 and 5 km (900 and 600 hPa). This may be
725 related to subsidence behind the propagating MJO. Nevertheless, it does demonstrate how
726 dynamics in the Indian Ocean and the formation of dry layers can be coupled to SCS/ES and
727 Sulu Sea convection and their aerosol environment. In regard to upper-level subsidence,
728 trajectories are highly divergent, but show significant lifting and subsidence associated with the
729 passage of TCs.

730

731 *4.2 High Frequency Squall Line and Cold Pools Phenomenon*

732 Embedded in the Figure 7 time series are clear, sharp perturbations in both meteorological and
733 aerosol features. Most significant of these are drops in temperature on the order of 2-5 °C within
734 minutes, and even here we must consider the response time of the aspirated temperature probe.
735 With the drop in temperature, there was a sharp spike in wind speed, relative humidity and at
736 times precipitation, and a drop in particle concentration and water vapor mixing ratio. These
737 characteristics are indicative cold pool events related to convective downdrafts (*Wakimoto* 1985;
738 *Atkins and Wakimoto* 1991; *Miller et al.*, 2008; *Zuidema et al.*, 2012). Over twenty such events
739 are observable in the time series, with significant variability in amplitude. Recovery from the
740 drop in temperature and particle concentration to the pre-event baseline ranged from one to ten
741 hours. Some of these events originated from what were clearly local isolated cells. However,
742 investigation of the largest such events suggest that they originate in long-lived squall lines,
743 propagating in the monsoonal flow and initiated from the cold pools of massive thunderstorms
744 over land or along the coast. This phenomenon appears to be extremely important for
745 determining aerosol fate in this region, and deserves detailed study in its own right. For this
746 study, we will limit our discussion to the most significant event observed during the cruise.

747

748 The pathology of SCS/ES organized squall line/cold pool phenomena best described by the
749 cruise data was for a Sept 24th event in the middle of the first significant aerosol transport
750 episode. Key aspects of the Sept 24th event are presented in Figure 10 as one-minute averages.
751 Included are (a) a time series of temperature and wind speed; (b) relative humidity and pressure;
752 (c) PCASP and CPC total particle count; and PCASP (d) number and (e) volume size
753 distributions. The cold pool hit at 16:28 UTC (corresponding to 00:28 LST on Sept 25th). Wind
754 cup speed accelerated from the background 7-8 m s⁻¹ to 14 ms⁻¹ within the first two seconds, with
755 flux estimates of gusts at the two-to-five second level to 25 m s⁻¹ within the next fifty seconds.
756 Winds then momentarily subsided to 5 ms⁻¹ for the next ten minutes, followed by another
757 increase and decrease over the next hour, and a slow recovery. Corresponding with the wind
758 onset was a ~5°C drop in temperature, and increase in relative humidity over the first minutes,
759 although there was only a minor 0.2 hPa perturbation in pressure. Sea surface temperature
760 dropped 0.2°C and recovered only after sunrise. Approximately 1 cm of precipitation occurred
761 over a one-hour period, initiated fifteen minutes after gust front arrival, breaking the wind lull.
762 Maximum precipitation rate was on the order of 4 cm hr⁻¹. Surface particle concentrations
763 dropped precipitously with cold pool arrival: PCASP counts dropping from ~700 cm⁻³ to 300 cm⁻³
764 ¹ within two minutes, followed by a further reduction to 150 cm⁻¹ at precipitation onset. CPC
765 dropped from ~1450 to 400 cm⁻¹. An interesting feature was a clear enhancement in coarse-mode
766 sea salt along the gust front. This is, to our knowledge, a first ever report of a maritime corollary
767 to dust producing haboobs (Knippertz et al., 2007; Miller et al., 2008; Seigel and van den
768 Heever, 2012). Particles and meteorological parameters likewise recovered to pre-event levels
769 over the next ten hours.

770

771 While the Sept. 24th event was the largest of its kind, it nevertheless demonstrated patterns
772 similar to over twenty other events: a sharp wind increase and temperature and particle decrease
773 is followed by a lull and eventually precipitation from a cell. When these events occurred in
774 association with isolated cells, we often could observe the entire process from cell formation to
775 cold pool onset and, at times, cell propagation over the site. Investigation of the Sept 24th case,
776 however, led us to a conclusion that despite the short spatial and temporal timescales observed at
777 a receptor site such as the *Vasco*, they are part of a meteorological phenomenon that spans the
778 entire SCS/ES region. Visible and IR satellite imagery of the SCS/ES region for the eighteen

779 hours prior to the September 24th event are presented in Figure 11. At arrival, the cell was only
780 30-50 km along the meridian, with cloud top heights on the order of 12-13 km, well below the 18
781 km tropopause height. Tracing the event back in time with fifteen-minute imagery, we found this
782 system, despite its small size, remained organized for nearly twenty-four hours. Imagery suggests
783 that an isolated thunderstorm that formed near the southern tip of Vietnam/Ho Chi Min City
784 initiated a cold pool southward which eventually embedded within the Southwest monsoonal
785 flow. This cold pool triggered an arc cloud formation that triggered a new set of thunderstorms
786 along the arc, which in turn formed a secondary cold pool and repeated.

787
788 Squall line features such as observed here have been long noted in the literature (e.g., *Trier et al.*,
789 1996), although we have been unable to find cases as long-lived as we found during the cruise.
790 There are some similarities in the radar science literature for mid-latitude systems as “bow
791 echoes” (*Weisman*, 1993). The physics have been studied extensively (e. g., *Weisman and*
792 *Rotunno*, 2004), and the importance of vertical wind shear and the presence of mid-tropospheric
793 dry air behind the storm front is well established. However, the nature of the squall lines in the
794 SCS/ES appears to present an extreme case. Figure 11 (g) and (h) show the MODIS Aqua 670
795 nm visible and cloud top height products for the Sept. 24th event, ten hours before it reached the
796 *Vasco*. Shown is a pair of squall lines, with the southern arc being the one that eventually
797 developed most strongly. We find it interesting that, for the most part, the tops of the clouds
798 making up the squall lines reached only 5-6 km, and hence were most likely ice-free. Only
799 isolated cells along the arc became high enough for freezing and further vertical development.
800 However, a review of the satellite loop suggests periodic major storm eruptions along the line,
801 which we surmise help propagate the phenomenon. In comparison, classic mid-latitude bow
802 echoes are very deep along the front; the difference in cloud heights may be related to the
803 relatively larger amounts of CAPE aloft in mid-latitude systems (*Takemi*, 2014), as well as the
804 location of the capping inversion. Long-lived squall lines are known to develop in environments
805 with finely tuned balance between shear and CAPE (*Rotunno et al.*, 1988). The question of
806 whether cold pool propagation is drive by the frequent and relatively shallow convection or the
807 infrequent troposphere-deep convection is one we plan to study in detail in the near future. From
808 an aerosol point of view, the warm versus cold convective components along the line likely have
809 important ramifications for scavenging or redistribution of aerosol particles in the MBL.

810 Similarly, aerosol impacts on warm versus cold convection are likely different. Aerosol particles
811 have even been hypothesized to influence the cold pools themselves (*Lebo et al.*, 2014).

812
813 A second important aspect of these cold pools is their extent across the monsoonal flow. The case
814 experienced by the *Vasco*, while long-lasting, was relatively small in dimension. Frequently,
815 much larger events are observed in our analysis of the satellite data record. An example at the
816 beginning of the research cruise (Sep 18) is presented in Figure 11(i). In this case, younger and
817 more developed squall lines are shown, each over 500 km in length. These events were initiated
818 by major thunderstorms over and just offshore of the Malay Peninsula, with overshooting tops of
819 >20 km. They propagated across the entirety of the SCS/ES in under thirty hours. With such
820 wide ranging extent, they must have swept across the entirety of the SCS/ES, perhaps leaving the
821 very clean condition observed in the northern area. Imagery analysis showed the southern
822 portions of these squall lines developing more strongly on their southern half. This suggests that
823 indeed the veering wind shear is supplying energy from the southern domain.

824

825 *4.3 Key Aspects of Chemistry and Particle Microphysics*

826 Detailed analysis of aerosol chemistry, size, and optical properties will be presented in
827 subsequent papers. However, there are key aspects of chemistry and size worth briefly discussing
828 in the context of this regional aerosol source and transport paper. Time series of DRUM sampler
829 derived PM₁ for some key elements are presented in Figure 12: (a) sulfur and potassium and (b)
830 aluminum and vanadium, respectively. Key gas species of CO and benzene are presented in
831 Figure 12(c) as is 2-PenONO₂ (a photo-oxidation product for pentane) and methyl iodide (CH₃I)
832 a marker for biomass burning (*Akagi et al.*, 2011). While aerosol source identification in the
833 complex Southeast Asian environment can be very involved (see e.g. *Atwood et al.*, 2013), there
834 are significant features of note. First, though non-sea salt sulfur can be produced by both
835 industrial and biomass burning (particularly peat burning for sulfur), potassium shows significant
836 enrichment during flaming biomass burning (*Reid et al.*, 2005; *Akagi et al.*, 2011). While aerosol
837 source identification in the complex Southeast Asian environment can be very involved (see e.g.
838 *Atwood et al.*, 2013), there are significant features of note. First, though non-sea salt sulfur can
839 be produced by both industrial and biomass burning (particularly peat burning for sulfur),

840 potassium shows significant enrichment during flaming biomass burning (*Reid et al.*, 2005;
841 *Akagi et al.*, 2011).

842
843 By and large, sulfur and potassium track with each other over the time period, with a significant
844 enrichment in the post-TC Nesat clear area. Aluminum, indicative of regional fine dust, or at
845 times fly ash, also tracks sulfur well and potassium quite well, perhaps indicative of soils
846 entrained in biomass burning plumes. As an indicator of industrial or oil combustion, vanadium
847 shows two significant spikes on Sept 26 and Sept 30. This may indicate additional industrial or
848 shipping sources. Based on our trajectory analysis, these cases may very well be influenced from
849 the industrial Singapore-Kuala Lumpur corridor, although high-resolution modeling is required
850 to show this with any certainty. From a gas chemistry point of view, we find that fine aerosol and
851 CO match reasonably well, with the CO enrichment ahead of the Sept 24-26 aerosol event
852 perhaps indicative of polluted air masses where particles have been scavenged by precipitation.
853 Benzene, a good and relatively stable indicator of biomass burning and some industrial
854 emissions, also tracks CO, though with perhaps less enrichment in the last day of the cruise.
855 Methyl iodide tracks with potassium as we would expect from a biomass burning tracer. As 2-
856 PenONO₂ is a photo oxidation product, its presence demonstrates that these plumes are
857 nominally well aged, particularly for the first event. A reduction in 2-PenONO₂ for the last day
858 of the cruise with an enhancement vanadium suggests a change in air mass sources and/or aging.
859 At the same time, the ratio of Ethyne to excess CO can also be used as a photochemical clock for
860 plume aging. While relatively noisy from the cruise, it ranged from 15 for the Sept 18 spike
861 suggesting a fresh source, was consistently lower (2 to 5) for the Sept 28-30 event suggested
862 uniformity in fair degree of photochemical aging. Conversely, the Sept 24-26 event showed
863 more variability (3 to 8), suggesting more mixed photochemical aging and perhaps sources. Such
864 chemistry must be further analyzed with the aid of numerical models.

865
866 Regarding aerosol size properties, fine-mode size distributions exhibited some variability
867 throughout the cruise (Figure 12; Table 1). Number distributions showed relatively strong trends,
868 with cleaner periods having significantly smaller count modal diameters (~0.11 to 0.24), though
869 curve fits generally converged to count median diameters in the 0.13-0.17 range. Implicit in this
870 is variability in geometric standard deviation, which may have significance in regional aerosol-

871 cloud condensation nuclei studies. Also evident in the number distributions is a frequent shoulder
872 on the large side of the distribution, suggesting differences in aerosol physics and chemistry for
873 the number and volume distributions; not uncommon in mixed environments. Volume median
874 diameters were generally in the 0.27-0.29 μm range for more polluted events, further exhibiting
875 larger overall size. Actual volume modal diameters are slightly larger (~ 0.02) than their curve-fit
876 counterparts. These are typical for both regional pollution and biomass burning environments
877 (*Reid et al.*, 2005; 2013), and are comparable to the AERONET derived VMDs by *Salinas et al.*,
878 (2013) of 0.26-0.40 μm for background and severe smoke haze events and the mean value of
879 0.32 μm by *Reid et al.* (2013) when one considers hygroscopicity.

880
881 An interesting aspect of the particle size and chemistry data for high-frequency events is
882 exemplified by the Sept. 24th cold pool case. Selected thirty-minute average volume distributions
883 taken from the one-minute time series in Figure 10(e) are presented in Figure 13 (c). Thirty-
884 minute average volume distributions leading up to the cold pool event, and twenty-four hours
885 later are nearly identical. In the ten minutes after arrival, we find a $\sim 80\%$ reduction in total
886 particle volume, with another factor of two reduction following the precipitation event. All this
887 time, VMDs remained fairly stable, although a clear increase in larger particle concentrations is
888 observed post wind burst. Between Figure 13 (c) and Figure 10 (d) & (e) we do not see large
889 changes in particle size, but rather only in amplitude. Similarly, ratios of aerosol chemistry are
890 also fairly similar. We can interpret this data and the seven hours before initiation of aerosol
891 population recovery as a sweep of clean air aloft and subsequent further rainout of aerosol
892 particles along the cold front. Given the 3-4 m/s^{-1} marine boundary layer wind speed, over seven
893 hours we expect a roughly 75 km zone of marine boundary layer particles being cleaned out by
894 the event upstream of the *Vasco*. Such a length scale is supported by the satellite images
895 presented in Figure 11, suggesting a ~ 120 -160 km swath was cut by the event.

896 897 5.0 DISCUSSION AND IMPLICATIONS FOR CLOUD and PRECIPITATION STUDIES

898 This paper had three primary objectives: 1) provide a broad overview of the 2011 *Vasco* cruise,
899 including instruments carried, cruise track, and the general characteristics of the regional
900 environment sampled; 2) relate how aerosol properties co-varied with regional meteorological
901 phenomenon and establish the extent to which biomass burning or industrial pollution from the

902 southern Maritime Continent can be transported towards or into the boreal summer southwest
903 monsoonal trough; and 3) create a narrative based on field data to help bridge climatological
904 indicators commonly used to assess aerosol lifecycle to real world meteorology. To our
905 knowledge, these are the first published aerosol field measurements in the boreal summertime
906 SCS/ES region.

907

908 Central to all meteorological and atmospheric compositional questions for the greater Maritime
909 Continent is the role of convection. As discussed in *Reid et al.* (2012; 2013), if ENSO-induced
910 precipitation anomalies influence the overall interannual variability of burning activity, it is the
911 patterns of convection correlated with MJO indices that best describe the specific timing and
912 lifetime of emissions. Indeed, the importance of the MJO to meteorological phenomenon of the
913 MC cannot be understated (*Zhang, 2014*). Yet we understand very little of the mechanisms of
914 MJO propagation across the region. Embedded in the large scale “forest” point-of-view of
915 ENSO, monsoonal transitions, and the MJO are individual “trees” of specific aerosol and
916 convective events that can be quite diverse in nature, resulting in complex relationships across
917 land, ocean and atmospheric processes.

918

919 From the “forest” point of view, the *Vasco* observed aerosol and meteorology phenomena that
920 largely matched the conceptual model of MC aerosol relationships between fire activity,
921 transport and MJO transport put forth in *Reid et al.* (2012). The entire 2011 burning season was
922 represented by fire activity slightly elevated with what one expects from a moderately-cold
923 ENSO year. Timing of specific burning events was largely consistent with drier phases of the
924 MJO for the western MC (Phases 1 and 5-7). The cruise fortunately took place during an MJO
925 propagation from 3 into 6, and towards the end of a significant burning event, and so sampled
926 some very clean air as well as the highest AOT recorded in the region for that season (Marbel
927 University Mindanao peaked at 500 nm AOT of 0.46, likely as a receptor for southern
928 Kalimantan burning on Sept 28th).

929

930 At the next level of scale, the migration of the MJO into phase 5 around Sept 22 coincided with
931 the development of regional TCs, as described by *Maloney and Hartman* (2001). This included
932 the early-cruise development of a TC in the SCS/ES and the pair of late cruise Category 4 TCs

933 propagating westward across Luzon at the very end of the mission. These TCs clearly enhanced
934 convection along a 2500 km inflow arm spanning the Sumatra/Malay Peninsula to Luzon, and
935 yet also are apparently associated with clear periods and rapid aerosol transport. Indeed, the
936 inflow arm that creates convection, and hence wet deposition, can, at the end of its lifecycle,
937 perhaps rapidly carry more polluted air masses into the SCS/ES and Sulu Seas. In these cases,
938 smoke and anthropogenic emissions from Sumatra and Borneo flowed deep into the greater
939 SCS/ES and Sulu Sea regions. It is quite possible that without TC influence, such events would
940 never have been observed. *Control for TC activity is a likely necessity in any climatological*
941 *analysis of regional aerosol transport.*

942
943 At the finest scales, we were impressed by the nature of coherently-propagating squall line
944 systems across the SCS/ES region, and how these perhaps cut large swaths of aerosol particles
945 out of the environment. Even a cursory view of geostationary data in Fig. 11 shows how
946 convection moves along isolated lines embedded in the SCS/ES monsoonal flow. These features
947 are contrary to the more “bubbling pot” concept of tropical convection in large-scale waves.
948 Examining the entire mission data record, we tracked dozens of lines of convection on the order
949 of 100-500 km in latitudinal length, propagating eastward. Cold pools of storms clearly initiate
950 new convection, which forms another set of cold pools and so on. Veering wind shear allows
951 these storms to cut across aerosol particles transported in the marine boundary layer, effectively
952 removing them from that altitude regime. Perhaps the dry air intrusions in the lower free
953 troposphere from the Indian Ocean provides needed dry air to perpetuate the bow echo-like form
954 observed. But this is speculative at this time and much more research is needed on the physics
955 and conditions that support long squall line phenomenon.

956
957 From an aerosol point of view, the prevalence of high-resolution features like cold pools, and the
958 warm versus cold convective components along the line, likely have important ramifications for
959 scavenging and/or redistribution of aerosol particles in the MBL. Aerosol particles have even
960 been hypothesized to influence the cold pools themselves (*Lebo et al., 2012*), offering up a
961 potential feedback. While there have been many attempts to correlate convective activity with
962 aerosol indicators, such as AOT, organized squall line behavior such as presented here will defeat
963 such a methodology. In the Sept 24th case, the high winds of the cold pool were ahead of the

964 precipitating cell. Thus, particle concentrations were dramatically reduced before the cell arrived.
965 In a study of the influence of cold pool generated dust on the parent convective cell, *Seigel and*
966 *van den Heever* (2012) found the dust had little effect. Vertical transport of the dust was
967 harmlessly ingested at mid-levels. No doubt, the burst of sea salt produced by the cold pools
968 observed on the cruise would meet a similar fate. But, the findings of *Seigel and van den Heever*
969 (2012) have perhaps a more interesting corollary. If wind generated aerosol particles do not have
970 a significant effect, do the aerosol particles ahead of the cold pool also have a lesser effect? Are
971 these particles vertically redistributed and eventually entrained into the clouds at mid-levels as
972 well? Finally, what then is the role of vertical wind shear in bringing aerosol particles from the
973 south into the squall line convection? These questions on aerosol lifecycle and impacts relate
974 back to the convection physics and the nature of clouds within the squall line. From Figure 11(h),
975 cloud tops along the squall line are at 6 km or above, but the efficiency of aerosol scavenging by
976 these features is unknown, although we suspect they are important sinks for regional particles.

977

978 The strong relationships between convection patterns, emissions, and transport have serious
979 implications for regional study of aerosol impacts on clouds and precipitation. Even more so,
980 these process implications propagate further into climate change projections. While the studies of
981 Reid et al., (2012) and Xian et al., (2013) provide a good climatological foundation for aerosol
982 lifecycle, they are nevertheless a substantial smoothing of highly intricate ejection and
983 convection interactions. However, just because relationships are complex does not imply they
984 are fundamentally chaotic. While future papers will describe in more detail the covariance
985 between aerosol particles and convection, it is appropriate to close this paper recalling the
986 covariance between aerosol populations in the MBL and key features in atmospheric soundings
987 in Figure 8. Indeed, the presence of substantial amounts of smoke in the boundary layer is fully
988 intertwined with reduced convection and the presence of dry layers aloft-either through large
989 scale subsidence or dry air. At the same time, these dry layers likely influence the gross type and
990 structure of convection irrespective of aerosol particles as CCN. In future studies, we will
991 attempt to constrain aerosol causality components from thermodynamic forcing of regional
992 convection. At the heart of such an endeavor is understanding what controls convective
993 initiation. Clearly, any aerosol-precipitation study has to account for such complex meteorology.
994 Then, when one considers the implications of aerosol-precipitation feedbacks of a changing

995 climate, we must consider how such phenomenon as ENSO, monsoonal transitions, the MJO and
996 TCs will themselves change. For these phenomenon the community is already challenged to
997 perform medium range to seasonal forecasts, let alone develop consistent simulations in climate
998 models. Thus, perhaps the most important lesson of this work is that all aerosol-climate
999 interaction research for the region is predicated on further advancements of fundamental
1000 meteorological processes.

1001

1002 6.0 CONCLUSIONS AND HYPOTHESES FOR FUTURE WORK

1003 This paper provides a broad overview of the two-week research cruise of the *Vasco* for
1004 September 17-30, 2011 in the northern Palawan Archipelago of the Philippines. The ship was
1005 stationed on the windward side of the boreal summertime southwest monsoonal trough,
1006 influenced by Marine Boundary Layer (MBL) air originating from the islands surrounding the
1007 Java Sea. Lower free tropospheric air above the MBL largely originated in the Indian Ocean,
1008 passing through and over the Malay Peninsula. Based on the analysis of *Reid et al.* (2012), we
1009 suspected this region's MBL is impacted by anthropogenic pollution and biomass burning
1010 emissions from Indonesia, Malaysia, and Singapore. Given Southeast Asia's ubiquitous cloud
1011 cover, it is difficult to determine by remote sensing what the impact is of anthropogenic activities
1012 on aerosol populations in a region suspected to be vulnerable to aerosol impacts (*Reid et al.*,
1013 2013). What we do know is largely based on modeling studies, which have difficulty with this
1014 most complex of meteorological environments. Hence, this cruise provides the first ever, to our
1015 knowledge, contiguous measurements of the South China Sea/East Sea (SCS/ES) and Sulu Sea
1016 aerosol environment. Based on this cruise, and a subsequent one-month September 2012 *Vasco*
1017 cruise to be reported on later, we observed enough of the environment to study aerosol lifecycle
1018 and pose questions for targeted analysis and testing of cloud impacts. At the very least, the 2011
1019 cruise provides a narrative of real world meteorological phenomena to provide realistic
1020 conceptual models of how the regional aerosol lifecycle relates to the southwest monsoonal
1021 system. In summary, we reported on the following:

1022

1023 1) Boreal summertime 2011 was an El Nino/Southern Oscillation (ENSO) cold "La Nina"
1024 phase year, yet had slightly above-average burning activity for this inter-seasonal state. While

1025 peak burning and aerosol optical thicknesses (AOTs) on Sumatra and Borneo for 2011 occurred
1026 in mid-August, with > 0.8 fine mode 500 nm AOTs recorded by AERONET, the end of the *Vasco*
1027 cruise corresponded to the largest aerosol injection into the Philippines, bringing 500 nm fine
1028 mode AOTs on the order of 0.3 to 0.4.

1029

1030 2) The *Vasco* cruise corresponded with Madden Julian Oscillation (MJO) propagation from
1031 phase 2 to 6, which should enhance burning and transport (*Reid et al.*, 2012). With MJO
1032 propagation came significant tropical cyclone (TC) activity, including the formation of a tropical
1033 storm in the SCS/ES in the early part of the cruise (Haitang), and the propagation of two
1034 Category 4 storms at the very end (Nesat and Nalgae). This TC activity strongly modulated
1035 winds and convection in the greater SCS/ES and Sulu Sea, and thus aerosol regional transport
1036 and lifecycle.

1037

1038 3) Active convective phases associated with TC development and inflow arms demonstrated
1039 extraordinary clean conditions, with Condensation Particle Counter (CPC) concentrations as low
1040 as 150 cm^{-3} , although $300\text{-}500 \text{ cm}^{-3}$ were more typical. Corresponding non-sea salt fine-mode
1041 particle concentrations in these phases were $1 \text{ to } 3 \mu\text{g m}^{-3}$. Coarse sea salt was observed at $4\text{-}8 \mu\text{g}$
1042 m^{-3} . While CALIPSO data during the cruise is unavailable, we suspect that given the regional
1043 veering wind shear, highest particle concentrations were in the MBL. This is supported by
1044 NAAPS model data, as well as climatological analyses and analysis of CALIOP data from
1045 immediately after the cruise period.

1046

1047 4) In between TCs, two significant aerosol injection events were observed, each lasting ~ 2.5
1048 days. The first of these increased CPC particle concentrations to $\sim 1000 \text{ cm}^{-3}$, and average non-
1049 sea salt fine-mode particle concentrations to $\sim 8 \mu\text{g m}^{-3}$. We surmise that long-range transport of
1050 particles reduction of convection to allow long-range transport for this case was induced by a
1051 dry-air intrusion between 800-600 hPa ($\sim 2\text{-}4 \text{ km}$) from the Indian Ocean. This event is perhaps
1052 related to backside MJO subsidence and drying. The aerosol source of this event was likely
1053 southwestern Borneo or with some influence of southern Sumatra. A second more significant
1054 event, with CPC counts as high as 5000 cm^{-3} , occurred in the last days of the cruise when an area
1055 of very clear sky formed between two Category 4 TCs. In this case, significant upper-level

1056 subsidence brought dry air down to below 500 hPa (6 km). High winds in the final stages of the
1057 TC inflow arm leading up to this event may have had a role in its far reaching nature. This
1058 air mass was likely dominated by smoke ejection from southern through southeastern
1059 Kalimantan/Borneo, and perhaps the Sulu Sea. Veering vertical wind shear resulted in aerosol
1060 transport largely in the MBL.

1061
1062 5) While aerosol particle and gas chemistry are subjects of follow-on papers, there are clear
1063 biomass burning signals in both events, particularly in regard to K^+ , CO, benzene and methyl
1064 iodide in the second event. However, in general, air chemistry appears to be a mix of industrial
1065 pollution and biomass burning, with sulfur being the most significant element. Black carbon and
1066 organic carbon ranged from 2% for the cleanest periods, 5-7% for the aerosol events, and up to
1067 12% in Manila bay. Organic carbon was $\sim 30\%$, increasing to over 50% for the cleanest periods.

1068
1069 6) PCASP derived particle size distributions for more polluted cases was typical for a mix of
1070 pollution and biomass burning, with volume median diameters on the order of 0.27-0.30 μm .
1071 While the PCASP was inoperable for the cleanest periods, more background conditions in the
1072 early part of the cruise showed smaller VMDs, $\sim 0.21 \mu\text{m}$.

1073
1074 7) Frequent rapid decreases in particle concentration and temperature, with corresponding
1075 sharp perturbations in winds, were associated with cold pool events. Over twenty such cold pool
1076 events were observed during the cruise. We noted, however, that convection in the SCS/ES
1077 region is often associated with narrow squall lines propagating in the monsoonal flow. In the
1078 most significant case, convection was spawned by a severe thunderstorm over Ho Chi Min City,
1079 whose cold pool propagated southward. Once it reached the southwesterly monsoon, another set
1080 of convection was spawned, creating its own northeastward propagating event. Over the next
1081 twenty-four hours, multiple sets of convection repeated the cycle, leading to arc cloud formations
1082 extending 100-200 km in latitude propagating across the SCS/ES. Upon reaching the *Vasco*, a
1083 one-minute long high wind event (with up to 25 m s^{-1} instantaneous winds) coincided with a
1084 precipitous fall in fine-mode particle concentrations and simultaneous spike in coarse-mode sea
1085 salt. Satellite and measured recovery times suggested a 150 km swath was cut through the marine
1086 boundary layer by this event. While cells up to 20 km high are noted, much of the squall line is

1087 made up of nonfreezing clouds with tops of 6 km. Even a cursory view of regional satellite data
1088 shows these squall lines occur frequently in the southwest monsoonal flow. While only tens of
1089 km wide, they can extend 500 km long across the monsoonal flow, likely supported by low-level
1090 veering winds. These events likely cut swaths of aerosol particles out of the MBL and thus are
1091 likely a major driver of regional aerosol lifecycle. The observation of a cold pool well ahead of
1092 the convection must be considered in aerosol-convection interaction studies.

1093
1094 Based on the above observations, we discussed implications for aerosol, cloud, and precipitation
1095 interaction studies. While aerosol particles are clearly identified by the scientific community as
1096 having a critical role in cloud systems, the covariance between the presence of aerosol particles
1097 and the atmospheric boundary layer state creates an intertwined chicken and egg problem. The
1098 potential for confounding studies is significant. Aerosol injections into the SCS/ES and Sulu Sea
1099 regions were clearly modulated by MJO and TC phenomenon. Dry layers originating in the
1100 Indian Ocean influenced convection thousands of kilometers away. Such features have to be
1101 accounted for in any analysis. However, the significant cloud cover in the region makes data
1102 assimilation for key variables such as water vapor highly problematic. Aerosol observations also
1103 demonstrate substantial clear-sky bias. Higher resolution scales, such as for convection, impart
1104 important fine features and process that are not easily replicated in models. Ultimately, this
1105 investigation highlights how future studies need tight constraints on the overall meteorology,
1106 including high-frequency phenomena such as island ejection of smoke by the sea breeze and cold
1107 pools.

1108

1109 7.0 ACKNOWLEDGEMENTS

1110 Organization of this research cruise and associated land base collections required the assistance
1111 of a number of organizations, including the staff of the Office of Naval Research-Global program
1112 office and reservist unit (esp. Joseph Johnson, Blake McBride, Paul Marshall), the Manila
1113 Observatory (esp. Antonia Loyzaga and Fr. Daniel McNamara), US State Department/ Embassy
1114 in Manila (esp. Maria Theresa Villa and Dovas Saulys), and the Naval Postgraduate School (esp.
1115 Richard Lind). We are most grateful to the *Vasco* ship management and crew, managed by
1116 Cosmix Underwater Research Ltd, (esp. Luc Heymans and Annabelle du Parc). We are also
1117 grateful to the host institutions for regional AERONET site deployment and the use of derived
1118 optical thickness data herein. Figure construction was also assisted by Cindy Curtis (NRL) and
1119 Randy Johnson (UND). Funding for this research cruise and analysis was provided from a

1120 number of sources. Vasco time procurement was provided by the NRL 6.1 Base Program via an
1121 ONR Global grant to the Manila Observatory. Funding for NRL scientist deployment and
1122 instrument analysis was provided by the NRL Base Program and ONR 35. Remote sensing and
1123 model analysis was provided by the NASA Interdisciplinary Science Program. Reservist support
1124 was provided by ONR Program 38. The AERONET deployments were supported by the NASA
1125 Radiation Science Program. Gas chemistry was provided by the NASA Tropospheric Chemistry
1126 Program. Author JRC acknowledges the support of NASA Interagency Agreement
1127 NNG13HH10I on behalf of MPLNET and the SEAC⁴RS Science Team.

1128 8.0 REFERENCES:

- 1129 Akagi, S. K., Yokelson, R. J., Weidinger, C., Alvarado, M. J., Reid, J. S., Karl, T., Crouse, J.
1130 D., and Wennberg, P. O., Emission factors for open and domestic biomass burning for use
1131 in atmospheric models, *Atmos. Phys. and Chem.*, 11, 4039–4072, doi:10.5194/acp-11-
1132 4039-2011, 2011
- 1133 Anderson, T. L., Covert, D. S., Marshall, S. F., Laucks, M. L., Charlson, R. J., Waggoner, A. P.,
1134 Ogren, J. A., Caldow, R., Holm, R. L., Quant, F. R., Sem, G. J., Wiedensohler, A.,
1135 Ahlquist, N. A., and Bates, T. S., Performance characteristics of a high-sensitivity three
1136 wavelength, total, backscatter nephelometer, *J. Atm. Ocean. Tech.*, 13, 967-986, 1996.
- 1137 Atkins, N. T., and Wakimoto, R. M., Wet microburst activity over the southeastern United
1138 States: Implications for forecasting, *Weather Forecast.*, 6, 470– 482, 1991.
- 1139 Atwood, S. A., Reid, J. S., Kreidenweis, S. M., Cliff, S. S., Zhao, Y., Lin, N. H., Tsay, S.-C., Chu,
1140 Y.-C., and Westphal, D. L., Size resolved measurements of springtime aerosol particles
1141 over the northern South China Sea, *Atmos. Environ.*, 78, 134-143,
1142 doi:10.1016/j.atmosenv.2012.11.024, 2013a.
- 1143 Atwood, S. A., Reid, J. S., Kreidenweis, S. M., Yu, L. E., Salinas, S. V., Chew, B. N., and
1144 Balasubramanian, R., Analysis of source regions for smoke events in Singapore for the
1145 2009 El Nino burning season, *Atmos. Environ.*, 78, 219-230, doi:
1146 10.1016/j.atmosenv.2013.04.047, 2013b.
- 1147 Bond, T. C., Anderson, T. L., and Campbell, D., Calibration and intercomparison of filter based
1148 measurements of visible light absorption by aerosols, *Aerosol. Sci. Tech.*, 30, 582-600,
1149 doi: 10.1080/027868299304435, 1999.
- 1150 Cahill, T.A., Goodart, C., Nelson, J.W., Eldred, R.A., Nasstrom, J.S., and Feeny, P.J., Design and
1151 evaluation of the DRUM impactor, in: *Proceedings of the International Symposium on*
1152 *Particulate and Multiphase Processes*, Ariman, T. and Veziroglu, T. N. (Eds.), Hemisphere
1153 Publishing Corporation, Washington, D. C., 319-325, 1985
- 1154 Campbell, J. R., Reid, J. S., Westphal, D. L., Zhang, J., Tackett, J. L., Chew, B. N., Welton, E. J.,
1155 Shimizu A., and Sugimoto, N., Characterizing aerosol particle composition and the
1156 vertical profile of extinction and linear depolarization over Southeast Asia and the
1157 Maritime Continent: the 2007-2009 view from CALIOP, *Atmos. Res.*, 122, 520-543,
1158 doi:10.1016/j.atmosres.2012.05.007, 2013.
- 1159 Chang, C.-P., Ding, Y., Lau, N.-C., Johnson, R. H., Wang, B., and Yasunari T., (Eds.), *The Global*
1160 *Monsoon System: Research and Forecast*, 2nd Ed., World Scientific Publishers.,
1161 Singapore, 2011
- 1162 Chang, C.-P., Wang, Z., McBride, J., and Liu, C.-H., Annual cycle of Southeast Asia-Maritime
1163 Continent rainfall and asymmetric monsoon transition. *J. Climate* 18, 287-301, 2005

1164 Chew, B. N., Campbell, J. R., Reid, J. S., Giles, D. M., Welton, E. J., Salinas, S. V., and Liew, S.
1165 C., Tropical cirrus cloud contamination in sun photometer data, *Atmos. Environ.*, 45,
1166 6724-6731, doi: <http://dx.doi.org/10.1016/j.atmosenv.2011.08.017>, 2011

1167 Chew, B. N., Campbell, J. R., Salinas, S. V., Chang, C. W., Reid, J. S., Welton, E. J., Holben, B.
1168 N., and Liew, S. C., Aerosol particle vertical distributions and optical properties over
1169 Singapore, *Atmos. Environ.*, 79, 599-613, doi:
1170 <http://dx.doi.org/10.1016/j.atmosenv.2013.06.026>, 2013

1171 Chow, J. C., Watson, J. G., Pritchett, L. C., Pierson, W. R., Frazier, C. A., and Purcell, R. G., The
1172 DRI thermal/optical analysis system: Description, evaluation and applications in U.S. air
1173 quality studies, *Atmos. Environ.*, 27A, 1185–1201, 1993

1174 Cinco, T. A., de Guzman, R. G., Hilario, F. D., Wilson, D. M., Long-term trends and extremes
1175 in observed daily precipitation and near surface air temperature in the Philippines for the
1176 period 1951–2010, *Atmospheric Research*, 145–146, 12-26,
1177 <http://dx.doi.org/10.1016/j.atmosres.2014.03.025>. 2014.

1178 Clarke, A. D., and Kapustin V., N., The Shoreline Environmental Aerosol Study (SEAS): A
1179 context for marine aerosol measurements influenced by a coastal environment and long-
1180 range transport, *J. Atmos. Ocean. Tech.*, 20, 1351-1361, doi:
1181 [http://dx.doi.org/10.1175/1520-0426\(2003\)020<1351:TSEASS>2.0.CO;2](http://dx.doi.org/10.1175/1520-0426(2003)020<1351:TSEASS>2.0.CO;2), 2003

1182 Colman, J. J., Swanson, A. L., Meinardi, S., Sive, B. B., Blake, D. R., and Rowland, F. S.,
1183 Description of the analysis of a wide range of volatile compounds in whole air samples
1184 collected during PEM-Tropics A and B, *Anal. Chem.*, 73, 3723-3731, 2001

1185 Cruz, F. T., Narisma, G. T., Villafuerte, M. Q., Chua, K. U., and Olaguera, L. M., A
1186 climatological analysis of the southwest monsoon rainfall in the Philippines, *Atmos. Res.*,
1187 112, 609-616, doi:10.1016/j.atmosres.2012.06.010, 2013

1188 Draxler, R. R. HYSPLIT4 users' guide, last accessed March 2012, available at:
1189 <http://purl.access.gpo.gov/GPO/LPS47020>, 2004

1190 Draxler, R. R., and Hess, G. D., Description of the HYSPLIT_4 modeling system. NOAA Tech.
1191 Memo. ERL ARL-224, NOAA Air Resources Laboratory, Silver Spring, MD, 24 pp.,
1192 1997

1193 Draxler, R.R., and Hess, G.D., An overview of the HYSPLIT_4 modeling system of trajectories,
1194 dispersion, and deposition. *Aust. Meteorol. Mag.*, 47, 295-308, 1998

1195 Field, R.D., and Shen, S.S.P., Predictability of carbon emissions from biomass burning in
1196 Indonesia. *J. Geophys. Res.*, 113, G04024, doi:10.1029/2008JG000694, 2008

1197 Field, R.D., van der Werf, G.R., and Shen, S.S.P., Human amplification of drought-induced
1198 biomass burning in Indonesia since 1960, *Nat. Geosci.*, 2, 185-188,
1199 doi:10.1038/NCEO443, 2009

1200 Hamid, E.Y., Kawasakim, Z.-I., and Mardiana, T., Impact of the 1998-1998 El Niño event on
1201 lightning activity over Indonesia. *Geophys. Res. Lett.*, 28, 147-150, 2001

1202 Henintzenberg, J., Covert D. C., and Van Dingenen, R., Size distribution and composition of
1203 marine aerosols: a compilation and review, *Tellus B*, 52, 1104– 1122, 2000

1204 Holben, B. N., Eck, T. F., Slutsker, I., Tanre, D., Buis, J. P., Setzer, A., Vermote, E., Reagan, J. A.,
1205 Kaufman, Y. J., Nakajima, T., Lavenu, F., Jankowiak, I., and Smirnov, A., AERONET - A
1206 federated instrument network and data archive for aerosol characterization, *Remote Sens.*
1207 *Environ.*, 66, 1-16, 1998

1208 Hogan, T.F., and Rosmond, T.E., The description of the U.S. Navy Operational Global
1209 Atmospheric Prediction System's spectral forecast model, *Mon. Wea. Rev.*, 119, 1786-
1210 1815, 1991

1211 Hyer, E. J., and Chew, B. N., Aerosol transport model evaluation of an extreme smoke episode in
1212 Southeast Asia, *Atmos. Environ.*, 44, 1422-1427, doi:
1213 <http://dx.doi.org/10.1016/j.atmosenv.2010.01.043>, 2010

1214 Hyer, E. J., Reid, J. S., Prins, E. M., Hoffman, J. P., Schmidt, C. C., Miettinen, J. I., and Giglio,
1215 L., Patterns of fire activity over Indonesia and Malaysia from polar and geostationary
1216 satellite observations, *J. Atmos. Res.*, 122, 504-519, doi:10.1016/j.atmosres.2012.06.011,
1217 2013

1218 IPCC, Parry, M. L., Canziani, O. F., Palutikof, J. P., van der Linden, P. J., and Hanson, C. E.
1219 (Eds.): *Impacts, Adaptation, and Vulnerability, Climate change 2007*, Cambridge
1220 University Press, United Kingdom, 2007

1221 Joyce, R. J., Janowiak, J. E., Arkin, P. A., and Xie, P., CMORPH: A method that produces global
1222 precipitation estimates from passive microwave and infrared data at high spatial and
1223 temporal resolution, *J. Hydrometeorol.*, 5, 487-503, 2004

1224 Kahn, R. A., Nelson, D. L., Garay, M., Levy, R. C., Bull, M. A., Martonchik, J. V., Diner, D. J.,
1225 Paradise, S. R., Wu, D. L., Hansen, E. G., and Remer, L. A., MISR Aerosol product
1226 attributes, and statistical comparisons with MODIS, *IEEE T. Geosci. Remote*, 47, 4095-
1227 4114, 2009

1228 Kalnay, E., Kanamitsu, M., Kistler, R., Collins, W., Deaven, D., Gandin, L., Iredell, M., Saha, S.,
1229 White, G., Woollen, J., Zhu, Y., Leetmaa, A., and Reynolds, R., The NCEP/NCAR 40-
1230 year reanalysis project. *Bull. Amer. Meteor. Soc.*, 77, 437-471, doi:
1231 [http://dx.doi.org/10.1175/1520-0477\(1996\)077<0437:TNYRP>2.0.CO;2](http://dx.doi.org/10.1175/1520-0477(1996)077<0437:TNYRP>2.0.CO;2), 1996

1232 Knippertz, P., P., Deutscher, C., Kandler, K., Müller, T., Schulz, O., and Schütz L., Dust
1233 mobilization due to density currents in the Atlas region: Observations from the Saharan
1234 Mineral Dust Experiment 2006 field campaign, *J. Geophys. Res.*, 112, *D21109*,
1235 doi: [10.1029/2007JD008774](http://dx.doi.org/10.1029/2007JD008774), 2007

1236 Langner, A., and Siegert, F., Spatiotemporal fire occurrence in Borneo over a period of 10 years.
1237 *Global Change Biol.*, 15, 48-62, doi:10.1111/j.1365-2486.2008.01828.x, 2009

1238 Lebo, Z. J., and Morrison, H., Dynamical effects of aerosol perturbations on simulated idealized
1239 squall lines, *Mon. Wea. Rev.*, 142, 991-1009, doi: [http://dx.doi.org/10.1175/MWR-D-13-](http://dx.doi.org/10.1175/MWR-D-13-00156.1)
1240 00156.1, 2014

1241 Lee, S.-S., Feingold, G., and Chuang, P. Y., Effect of aerosol on cloud-environment interactions
1242 in trade cumulus, *J. Atmos. Sci.*, 69, 3607-3632. doi: [http://dx.doi.org/10.1175/JAS-D-](http://dx.doi.org/10.1175/JAS-D-12-026.1)
1243 [12-026.1](http://dx.doi.org/10.1175/JAS-D-12-026.1), 2012

1244 Madden, R. A., and Julian, P. R., Detection of a 40-50 day oscillation in the zonal wind in the
1245 tropical pacific, *J. Atmos. Sci.*, 28, 702-708, 1971

1246 Mahmud, M., Mesoscale model simulation of low level equatorial winds over Borneo during the
1247 haze episode of September 1997, *J. Earth Syst. Sci.*, 118, 295-307, 2009a

1248 Mahmud, M., Mesoscale equatorial wind prediction in Southeast Asia during a haze episode of
1249 2005, *Geofizika*, 26, 67-84, 2009b

1250 Maloney, E. D., and Hartman, D. L., The Madden Julian oscillation, barotropic dynamics, and
1251 the North Pacific tropical cyclone formation, part 1: Observations, *J. Atmos. Sci.*, 58,
1252 2545-2558, 2001

1253 Markowicz, K. M., Flatau, P. J., Kardas, A. E., Remiszewska, J., Stelmaszczyk, K., and Woeste,
1254 L., Ceilometer retrievals of the boundary layer vertical aerosol extinction structure, *J.*
1255 *Atmos. Ocean. Tech.*, 25, 928-944, 2008

1256 Miettinen, J., and Liew, S. C., Degradation and development of peatlands in Peninsular Malaysia

1257 and in the islands of Sumatra and Borneo since 1990, *Land Degrad. Dev.*, 21, 285-296,
1258 doi:10.1002/ldr.976, 2010

1259 Miettinen, J., Shi, C. H., and Liew, S. C., Deforestation rates in insular Southeast Asia between
1260 2000 and 2010, *Global Change Biol.*, 17, 2261-2270, doi:10.1111/j.1365-
1261 2486.2011.02398.x, 2011

1262 Miller, S. D., Hawkins, J. D., Kent, J., Turk, F. J., Lee, T. F., Kuchiauskas, A. P., Richardson, K.,
1263 Wade, R. and Hoffman, C., NexSat: Previewing NPOESS/VIIRS imagery capabilities.
1264 *Bull. Amer. Meteor. Soc.*, 87, 433–446, doi: <http://dx.doi.org/10.1175/BAMS-87-4-433>,
1265 2006

1266 Miller, S. D., Kuciauskas, A. P., Liu, M., Ji, Q., J. S. Reid, J. S., Breed, D. W., Walker, A. L., and
1267 Al Mandoos A., Haboob dust storms of the southern Arabian Peninsula, *J. Geophys. Res.*,
1268 113, D01202, doi:10.1029/2007JD008550, 2008

1269 Moron, V., Robertson, A.W., and Beer, R., Spatial coherence and seasonal predictability of
1270 monsoon onset over Indonesia, *J. Climate*, 22, 840-850, 2009

1271 Nichol, J., Smoke haze in Southeast Asia: A predictable recurrence, *Atmos. Environ.*, 32, 2715-
1272 2716, 1998

1273 O'Neill, N. T., Eck, T. F., Smirnov, A., Holben, B. N., and Thulasiraman, S., Spectral
1274 discrimination of coarse and fine mode optical depth, *J. Geophys. Res.*, 108, 4559,
1275 doi:[10.1029/2002JD002975](http://dx.doi.org/10.1029/2002JD002975), 2003

1276 Parungo, F., Boatman, J. F., Sievering, H., Wilkison, S. W., and Hicks, B. B., Trends in global
1277 marine cloudiness and anthropogenic sulfur. *J. Climate*, 7, 434-440, 1994

1278 Quinn, P. K., Kupustin, V. N., Bates, T. S., and D. S. Covert, Chemical and optical properties of
1279 marine boundary layer aerosol particles of the mid-Pacific in relation to sources and
1280 meteorological transport, *J. Geophys. Res.*, 101, 6931–6951, 1996

1281 Reid, J. S., Brooks, B., Crahan, K. K., Hegg, D. A., Eck, T. F., O'Neill, N., de Leeuw, G., Reid,
1282 E. A., and Anderson K. D., Reconciliation of coarse mode sea-salt aerosol particle size
1283 measurements and parameterizations at a subtropical ocean receptor site, *J. Geophys.*
1284 *Res.*, 111, D02202, doi:10.1029/2005JD006200, 2006

1285 Reid, J. S., Hyer, E. J., Prins, E. M., Westphal, D. L., Zhang, J. L., Wang, J., Christopher, S. A.,
1286 Curtis, C. A., Schmidt, C. C., Eleuterio, D. P., Richardson, K. A., and Hoffman, J. P.,
1287 Global Monitoring and Forecasting of Biomass-Burning Smoke: Description of and
1288 Lessons From the Fire Locating and Modeling of Burning Emissions (FLAMBE)
1289 Program. *IEEE J. Sel. Top. Appl.*, 2, 144-162, doi:10.1109/JSTARS.2009.2027443, 2009

1290 Reid, J. S., Reid, E. A., Walker, A., Piketh, S., Cliff, S., Al Mandoos, A., Tsay, S. C. and Eck, T.
1291 F., Dynamics of southwest Asian dust particle size characteristics with implications for
1292 global dust research, *J. Geophys. Res. Atmos.*, 113, D14212, doi:10.1029/2007JD009752,
1293 2008.

1294 Reid., J. S., Xian, P., Hyer, E. J., Flatau, M. K., Ramirez, E. M., Turk, F. J., Sampson, C. R.,
1295 Zhang, C., Fukada, E. M., and Maloney, E. D., Multi-scale meteorological conceptual
1296 analysis of observed active fire hotspot activity and smoke optical depth in the Maritime
1297 Continent, *Atmos. Chem. Phys.*, 12, 1–31, doi:10.5194/acp-12-1-2012, 2012

1298 Reid, J. S., et al., Observing and understanding the Southeast Asian aerosol system by remote
1299 sensing: An initial review and analysis for the Seven Southeast Asian Studies (7SEAS)
1300 program, *Atmos. Res.*, 122, 403-468, doi:10.1016/j.atmosres.2012.06.005, 2013

1301 Rotunno, R., Klemp, J. B, and Weisman, M. L.: A theory for strong, long-lived squall lines. *J.*
1302 *Atmos. Sci.*, 45, 463-485, 1988.

1303 Rosenfeld, D., TRMM observed first direct evidence of smoke from forest fires inhibiting
1304 rainfall, *Geophys. Res. Lett.*, 26, 3105–3108, doi:10.1029/1999GL006066, 1999

1305 Salinas, S. V., Chew, B. N., Mohamad, M., Mahmud, M., and Liew, S. C., First measurements of
1306 aerosol optical depth and Angstrom exponent number from AERONET's Kuching site,
1307 *Atmos. Environ.*, 78, 231-241, doi:10.1016/j.atmosenv.2013.02.016, 2013

1308 Seigel, R. B., and van den Heever, S. C., Dust lofting and ingestion by supercell storms, *J.*
1309 *Atmos. Sci.*, 69, 1453–1473, doi: <http://dx.doi.org/10.1175/JAS-D-11-0222.1>, 2012

1310 Smirnov, A., Holben, B. N., Giles, D. M., Slutsker, I., O'Neill, N. T., Eck, T. F., Macke, A.,
1311 Croot, P., Courcoux, Y., Sakerin, S. M., Smyth, T. J., Zielinski, T., Zibordi, G., Goes, J. I.,
1312 Harvey, M. J., Quinn, P. K., Nelson, N. B., Radionov, V. F., Duarte, C. M., Losno, R.,
1313 Sciare, J., Voss, K. J., Kinne, S., Nalli, N. R., Joseph, E., Krishna Moorthy, K., Covert, D.
1314 S., Gulev, S. K., Milinevsky, G., Larouche, P., Belanger, S., Horne, E., Chin, M., Remer,
1315 L. A., Kahn, R. A., Reid, J. S., Schulz, M., Heald, C. L., Zhang, J., Lapina, K., Kleidman,
1316 R. G., Griesfeller, J., Gaitley, B. J., Tan, Q., and Diehl, T. L., Maritime aerosol network as
1317 a component of AERONET – first results and comparison with global aerosol models and
1318 satellite retrievals, *Atmos. Meas. Tech.*, 4, 583-597, doi:10.5194/amt-4-583-2011, 2011

1319 Sorooshian, A., Feingold, G., Lebsock, M. D., Jiang, H., and Stephens, G. L., On the
1320 precipitation susceptibility of clouds to aerosol perturbations, *Geophys. Res. Lett.*, 36,
1321 L13803, doi:[10.1029/2009GL038993](http://dx.doi.org/10.1029/2009GL038993), 2009

1322 Takemi, T., Convection and precipitation under various stability and shear conditions: Squall
1323 lines in tropical versus midlatitude environment, *Atmos. Res.*, 142, 111-123.
1324 doi:10.1016/j.atmosres.2013.07.010, 2013

1325 Tian, B., Waliser, D. E., Kahn, R. A., Li, Q., Yung, Y. L., Tyranowski, T., Geogdzhayev, I. V.,
1326 Mishchenko, M. I., Torres, O., Smirnov, A., Does the Madden-Julian Oscillation
1327 influence aerosol variability?, *J. Geophys. Res.*, 113, D12215,
1328 doi:10.1029/2007JD009372, 2008

1329 Tosca, M. G., Randerson, J. T., Zender, C. S., Nelson, D. L., Diner, D. J., and Logan, J. A.,
1330 Dynamics of fire plumes and smoke clouds associated with peat and deforestation fires in
1331 Indonesia. *J. Geophys. Res.*, 116, D08207, doi:10.1029/2010JD015148, 2011

1332 Trier, S. B., Skamarock, W. C., LeMone, M. A., Parsons, D. B., Jorgensen, D. P., Structure and
1333 evolution of the 22 February 1993 TOGA COARE squall line: Numerical simulations, *J.*
1334 *Atmos. Sci.*, 53, 2861–2886, doi: [http://dx.doi.org/10.1175/1520-0469\(1996\)053<2861:SAEOTF>2.0.CO;2](http://dx.doi.org/10.1175/1520-0469(1996)053<2861:SAEOTF>2.0.CO;2), 1996

1336 Tsaknakis, G., Papayannis, A., Kokkalis, P., Amiridis, V., Kambezidis, H. D., Mamouri, R. E.,
1337 Georgoussis, G., and Avdikos, G., Inter-comparison of lidar and ceilometer retrievals for
1338 aerosol and Planetary Boundary Layer profiling over Athens Greece, *Atmos. Meas. Tech.*,
1339 4, 1261-1273, doi:10.5194/amt-4-1261-2011, 2011

1340 van der Kaars, S., Tapper, N., and Cook, E. J., Observed relationships between El-Nino Southern
1341 Oscillation, rainfall variability and vegetation and fire history on Halmahera, Maluku,
1342 Indonesia, *Global Change Biol.*, 16, 1705-1714. doi:10.1111/j.1365-2486.2009.02025.x,
1343 2010

1344 van der Werf, G. R., Randerson, J. T., Collatz, J., Giglio, L., Kasibhatla, P. S., Arellano Jr., A. F.,
1345 Olsen, S. C., and Kasischke, E. S., Continental-scale partitioning of fire emissions during
1346 the 1997 to 2001 El Niño/La Nina period, *Science*, 303, 73-76,
1347 doi:10.1126/science.1090753, 2004

1348 Wakimoto, R. M., Forecasting dry microburst activity over the High Plains, *Mon. Weather Rev.*,
1349 113, 1131– 1143, 1985

1350 Wang, J., Gei, C., Yang, Z., Hyer, E., Reid, J. S., Chew, B. N., and Mahmud, M., Mesoscale
1351 modeling of smoke transport over the South Asian maritime continent: vertical
1352 distributions and topographic effect, *Atmos. Res.*, 122, 486-503, 2013

1353 Weisman, M. L., The genesis of severe, long-lived bow echoes, *J. Atmos. Sci.*, 50, 645–670. doi:
1354 [http://dx.doi.org/10.1175/1520-0469\(1993\)050<0645:TGOSLL>2.0.CO;2](http://dx.doi.org/10.1175/1520-0469(1993)050<0645:TGOSLL>2.0.CO;2), 1993

1355 Weisman, M. L., and Rotunno, R., A Theory for Strong Long-Lived Squall Lines Revisited, *J.*
1356 *Atmos. Sci.*, 61, 361–382, doi: [http://dx.doi.org/10.1175/1520-0469\(2004\)061<0361:ATFSL>2.0.CO;2](http://dx.doi.org/10.1175/1520-0469(2004)061<0361:ATFSL>2.0.CO;2), 2004

1357

1358 Xian, P., Reid, J. S., Atwood, S. A., Johnson, R., Hyer, E. J., Westphal, D. L., and Sessions, W.,
1359 Smoke transport patterns over the Maritime Continent, *Atmos. Res.*, 122, 469-485,
1360 doi:10.1016/j.atmosres.2012.05.006, 2013

1361 Yuan, T., Remer, L. A., Pickering, K. E., Yu H., Observational evidence of aerosol enhancement
1362 of lightning activity and convective invigoration, *Geophys. Res. Lett.*, 38, L04701,
1363 doi:10.1029/2010GL046052, 2011

1364 Yusef, A. A., and Francisco, H., Climate change vulnerability mapping for Southeast Asia,
1365 Economy and Environment Program for Southeast Asia (EEPSEA) report, available at
1366 <http://www.eepsea.net>, last access July 2014, 32 pp, June 2009

1367 Zhang, C., Madden-Julian Oscillation, *Rev. Geophys.*, 43, RG2003,
1368 doi:10.1029/2004RG000158, 2005

1369 Zhang J. L., and Reid, J. S., An analysis of clear sky and contextual biases using an operational
1370 over ocean MODIS aerosol product. *Geophys. Res. Lett.*, 36, L15824,
1371 doi:10.1029/2009GL038723, 2009

1372 Zhang, J. L., Reid, J. S., Westphal, D. L., Baker, N. L., and Hyer, E. J., A system for operational
1373 aerosol optical depth data assimilation over global oceans, *J. Geophys. Res. Atmos.*, 113,
1374 D10208, doi:10.1029/2007JD009065, 2008

1375 Zhang, C., Madden-Julian Oscillation: Bridging Weather and Climate, *Bull. Amer. Meteor. Soc.*,
1376 94, 1849-1870, doi: <http://dx.doi.org/10.1175/BAMS-D-12-00026.1>, 2014

1377 Zuidema, P., Li, Z., Hill, R. J., Bariteau, L., Rilling, B., Fairall, C., Brewer, W. A., Albrecht, B.,
1378 and Hare, J., On trade wind cumulus cold pools. *J. Atmos. Sci.*, 69, 258–280, doi:
1379 <http://dx.doi.org/10.1175/JAS-D-11-0143.1> , 2012

1380

Table 1.

Date	Sample Location	Suspected Source	Mode:CMD: σ_{gn} (μm , μm , N/A)	Mode:VMD: σ_{gv} (μm , μm , N/A)	BC%/OC %	K/S
Sep. 16	Manila Harbor	Metro Manila			12%/19%	0.01
Sep. 17	Manila Bay	Local Bay	0.17:0.16:1.73	0.285:0.30:1.43		0.02
Sep. 17	Outside Manila Bay	Sulu Sea/N. Borneo	0.11/0.17 :0.13:1.37	0:19:0.21:1.52	Bdl/28%	0.08
Sep. 23	Malampaya Sound	Malay Pen. & Sumatra.	N/A	N/A	2%/58%	0.12
Sep. 25	El Nido	SW Borneo	0.17:0.17:1.61	0:285: 0.27:1.36	5%/27%	0.10
Sep. 29	N. El Nido	Southern Borneo	0.24:0.20:1.54	0.31:0.29:1.28	5%/30%	0.29
Sep. 30	Outside Manila Bay	N. Malay Pen. thru Vietnam	0:17:0.18:1.56	0.31:0.28:1.31	7%/31%	0.23

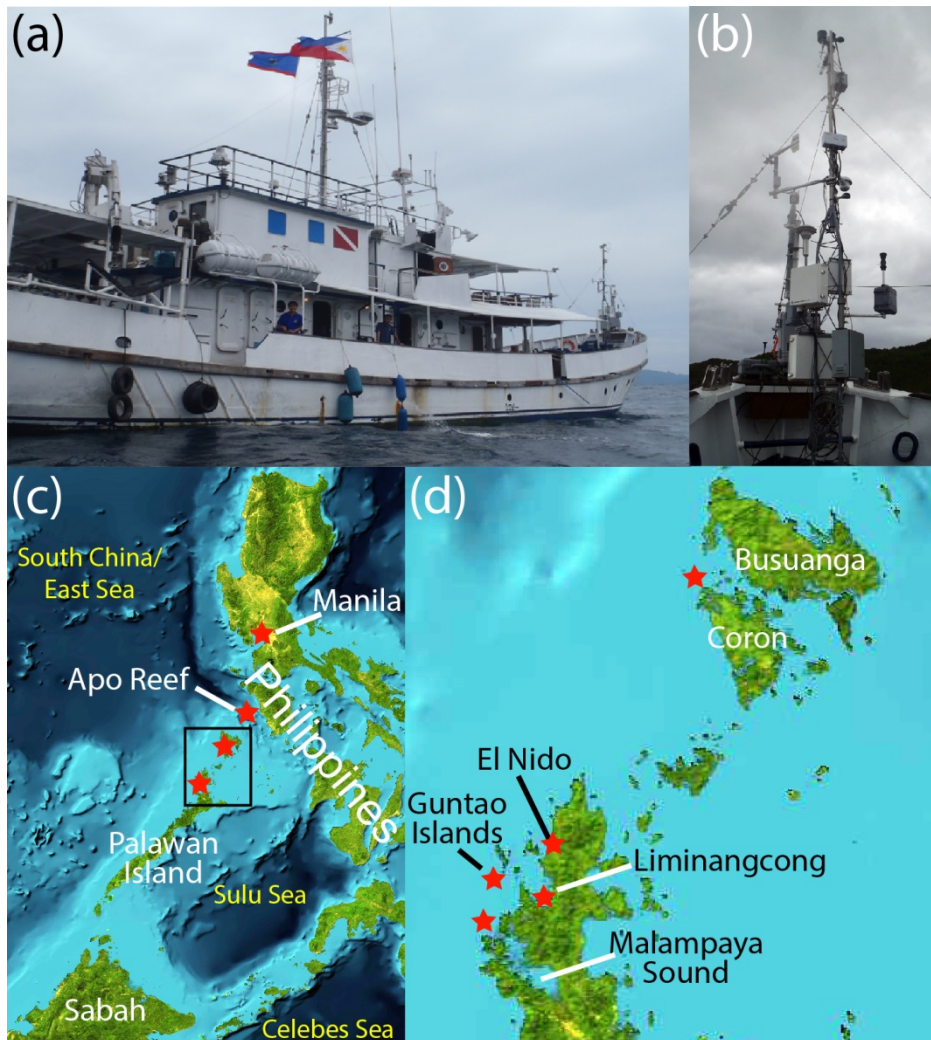


Figure 1. (a) The M/Y Vasco; (b) bow flux tower during the cruise. (c) Map of cruise area, stars mark key areas of sampling. (d) Enlargement of the northern Palawan/Coron Sampling sites.

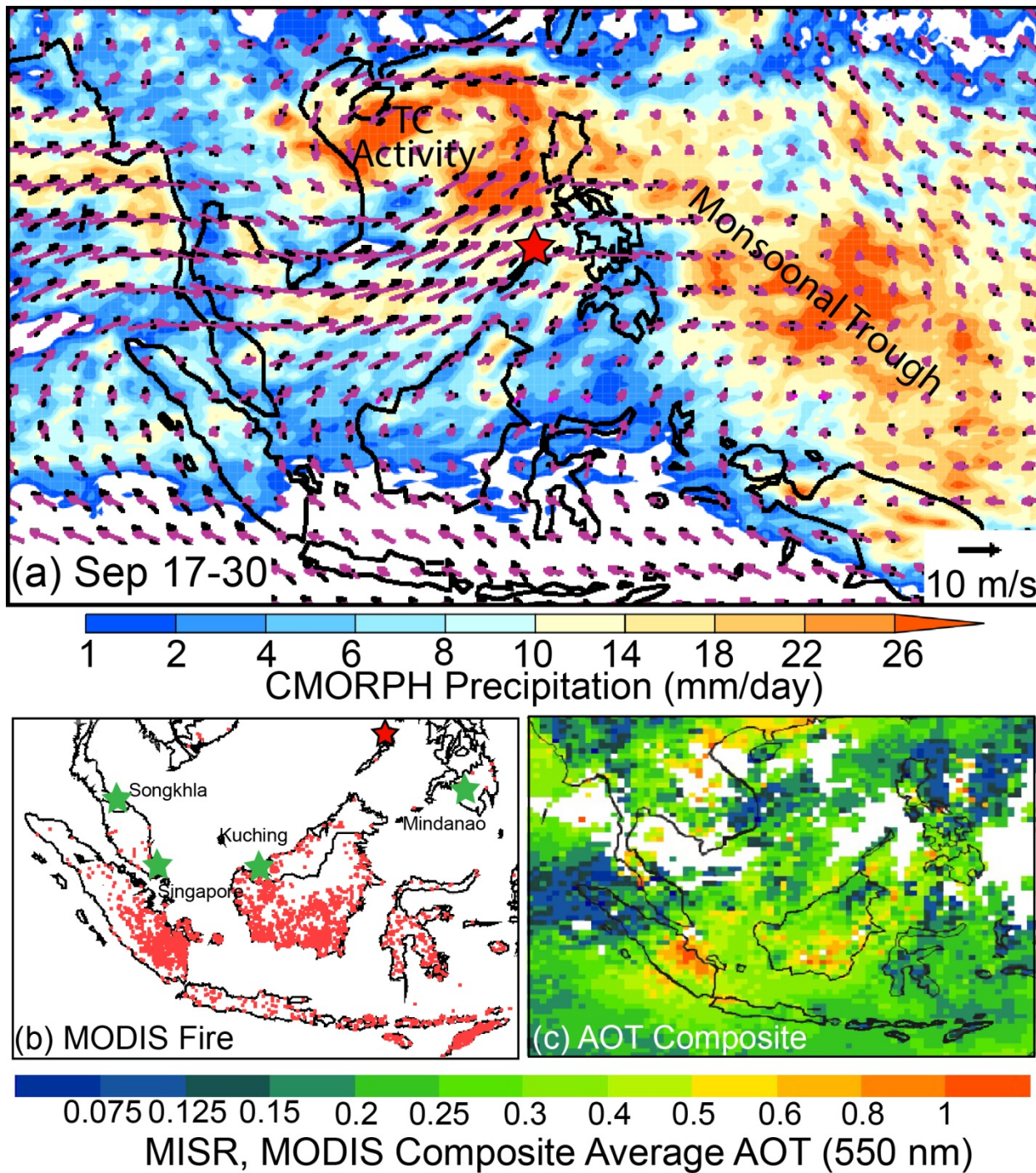


Figure 2. Overview of the aerosol and meteorological environment during the September 17-30 *Vasco* cruise. (a) Surface (black) and 850 hPa (purple) NOGAPS winds overlaid on CMORPH average precipitation rain rates. (b) MODIS Terra+Aqua active fire hotspot detections during the cruise. Overlaid in green stars are key AERONET locations. Red star depicts the El Niño receptor site sampled by the *Vasco*. (c) Composite average MODIS+MISR Aerosol Optical Thickness (AOT).

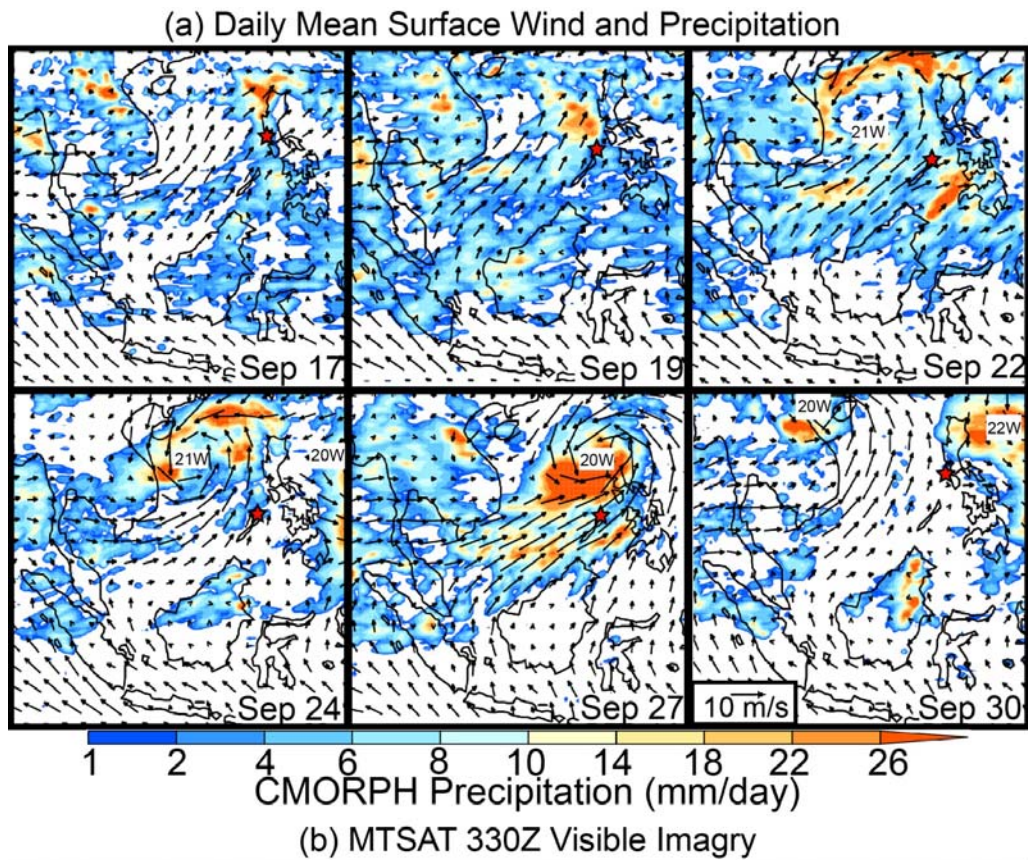


Figure 3. (a) Daily NOGAPS surface winds with CMORPH precipitation for 6 days throughout the cruise demonstrating key meteorological and aerosol modes. (b) Corresponding NexSat 330UTC/1130 LST MTSAT visible imagery with synthetic color background. Ship location at satellite imagery time is located by a red star.

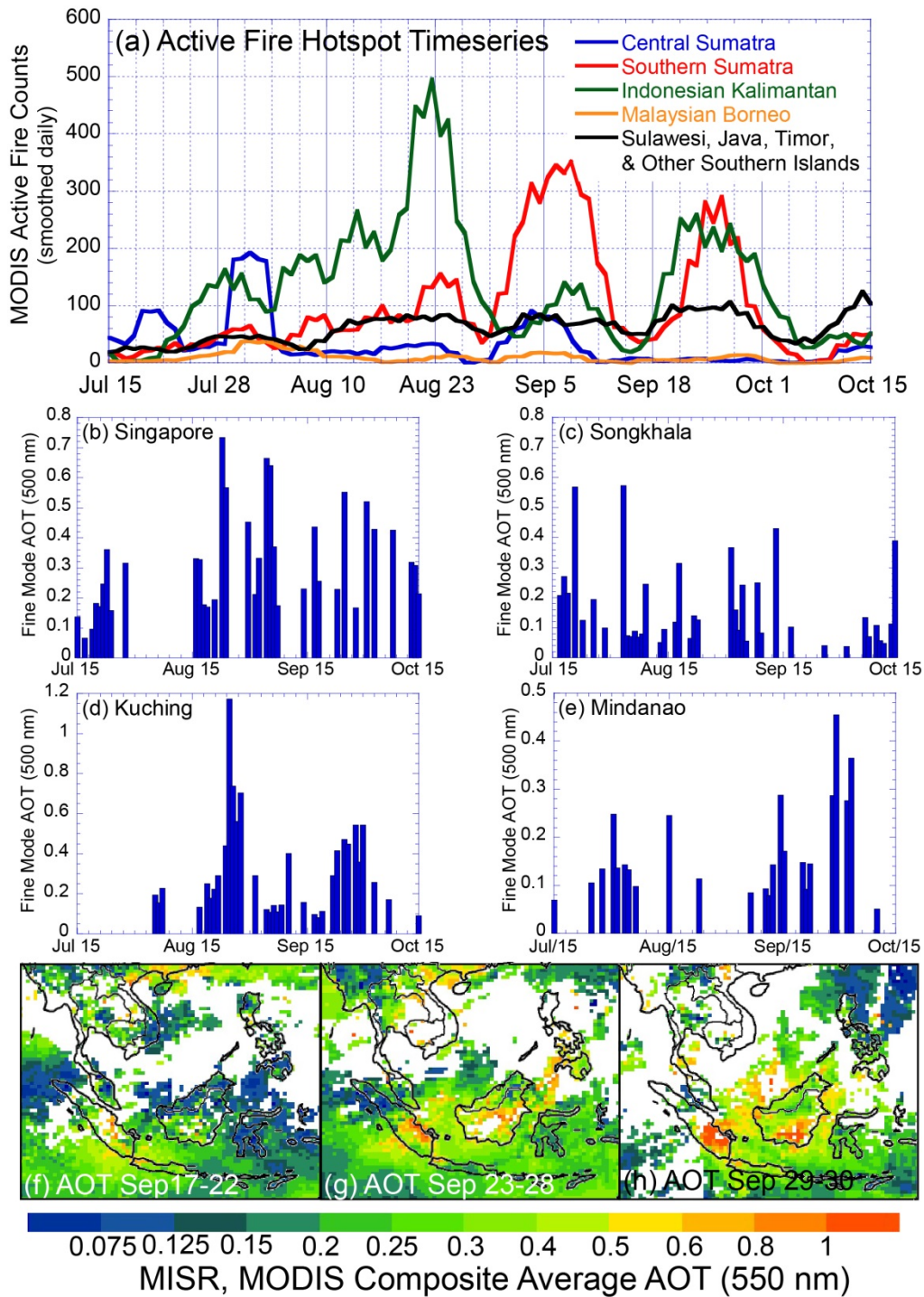


Figure 4. Contextual aerosol data for the 2011 aerosol season. (a) Combined MODIS active fire hotspot prevalence by region. Data is smoothed in a 5 day boxcar filter to help account for orbit. (b)-(e). Level 2 AERONET 500 nm fine mode AOTs for key sites in the Southeast Asian region (marked on Figure 2 (b)) (f)-(h) Combined MODIS 7 MISR satellite AOT analysis for the early, mid and late phases of the cruise.

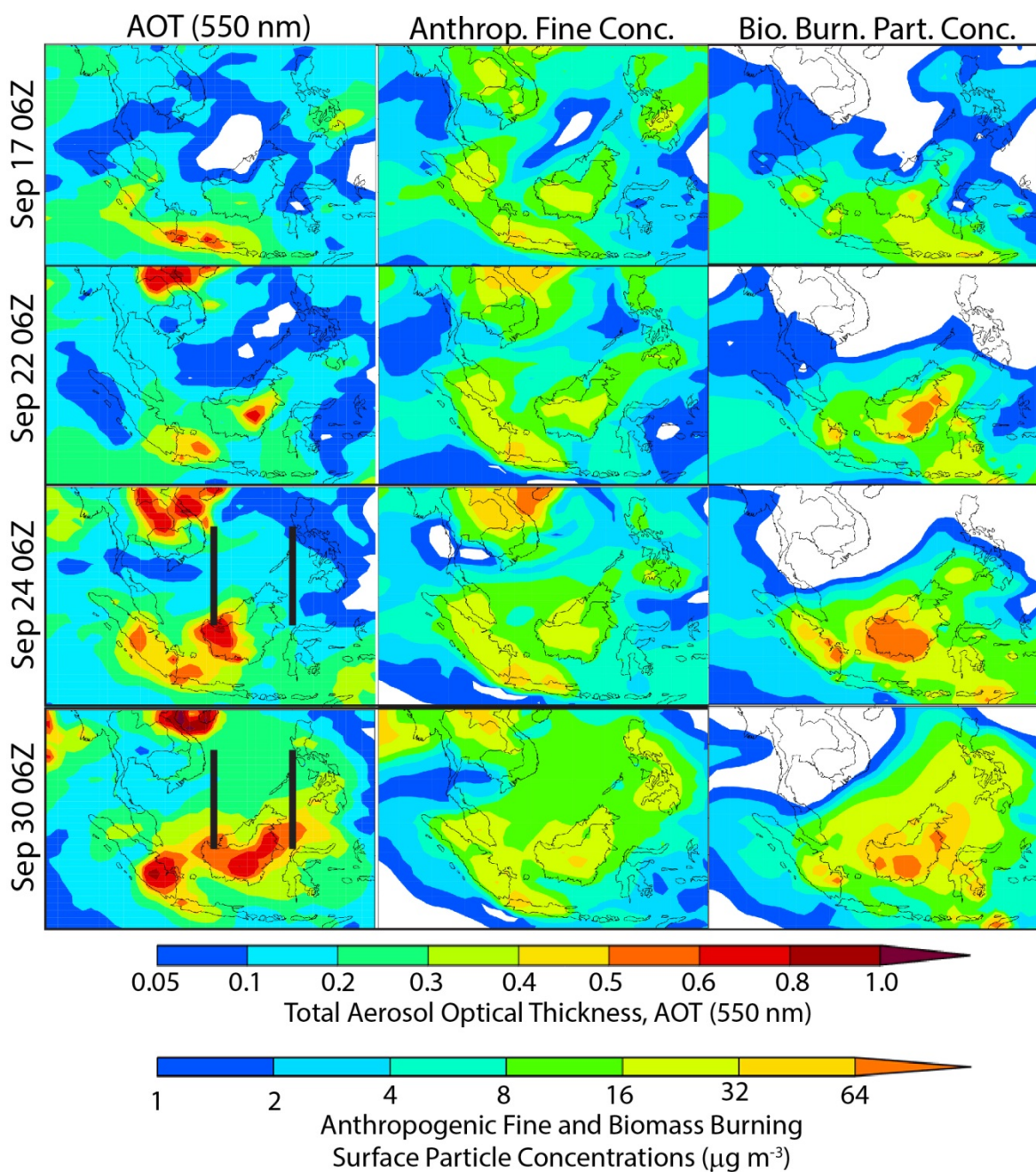


Figure 5. NAAPS 550 nm Aerosol Optical Thickness (AOT) and surface concentrations for fine mode anthropogenic and biomass burning particle concentrations for four key days during the cruise. Satellite data for these four days is also presented in Figure 3. Cross sectional lines for Figure 6 (Sep 24 and 30) are placed on the AOT plot.

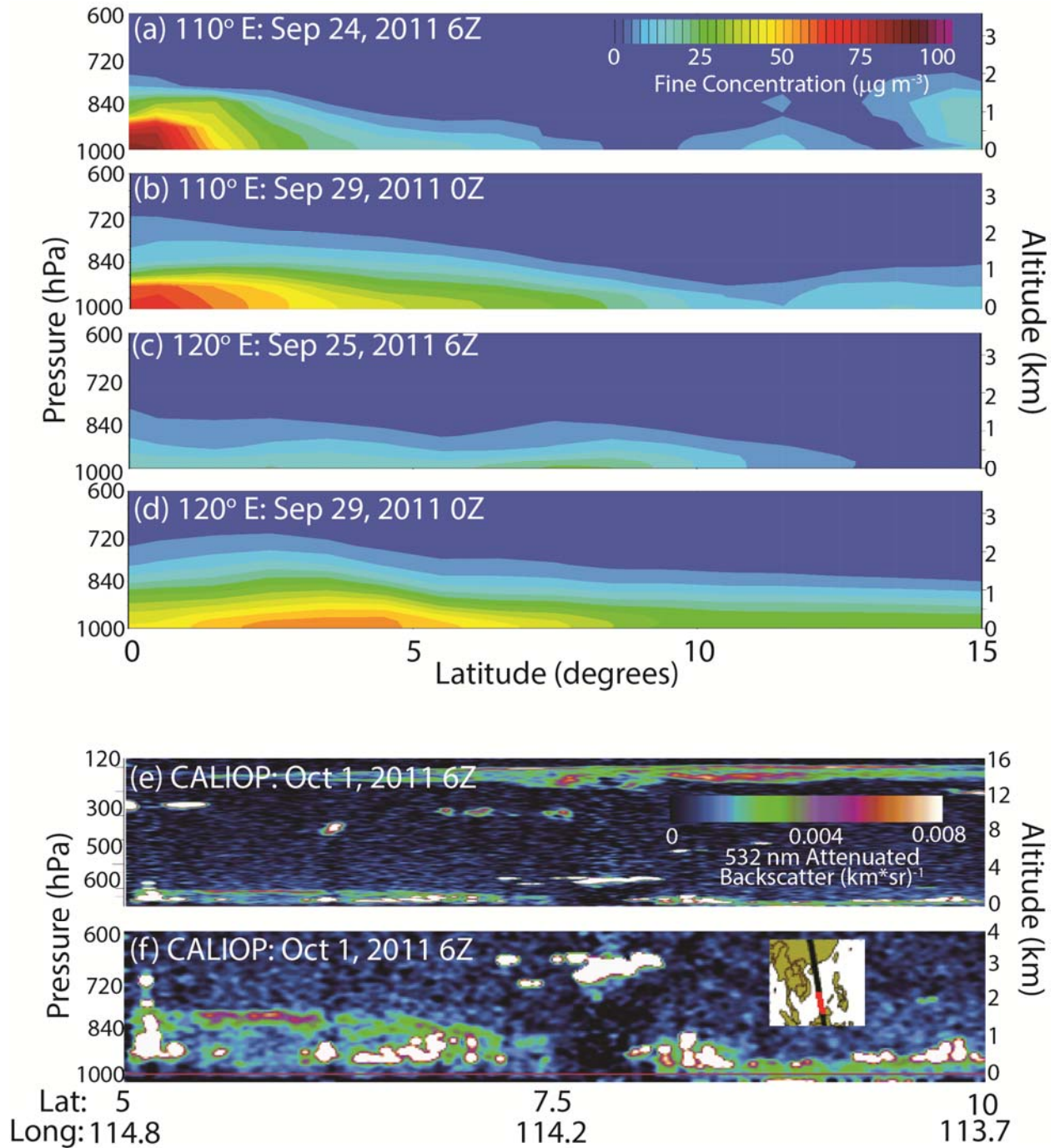


Figure 6. (a)-(d) Meridional cross sections at 110 and 120 east of NAAPS reanalysis total fine mode aerosol particle concentration for the September 25((a) and (c)) and September 29 ((b) and (d)) haze events. (e) CALIOP 532 nm backscatter across the SCS/ES region on Oct 1, 2011. (f) Rescaling of (e) for the lowest 4 km. Included is a map of the CALIPSO track.

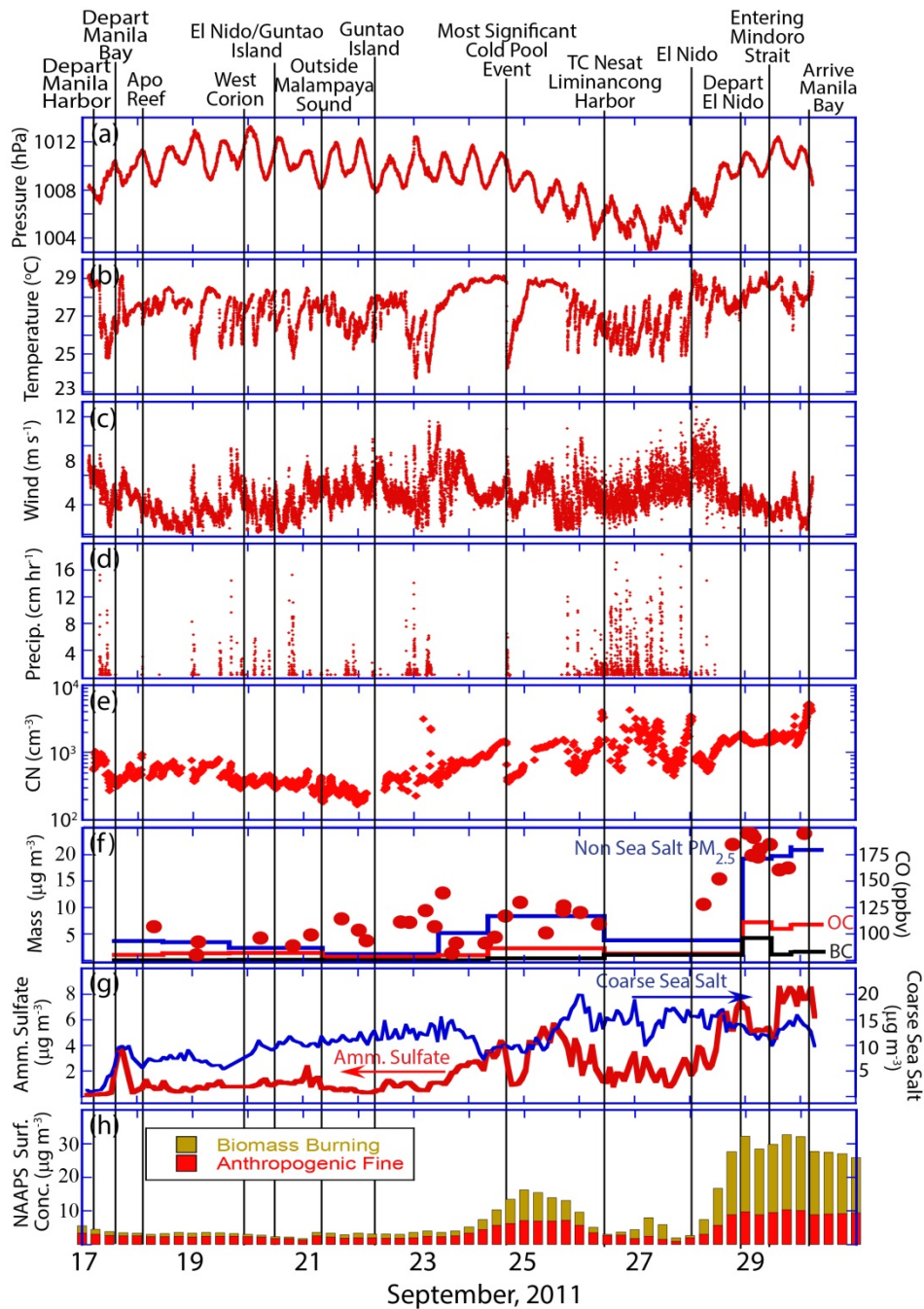


Figure 7. Cruise time series of key meteorological, aerosol and chemistry indicators in 1 minute intervals. Key sampling points and events are marked by vertical lines. (a) Surface pressure (hPa); (b) Ambient air temperature ($^{\circ}\text{C}$); (c) Wind speed (m s^{-1}); (d) Precipitation rate (cm hr^{-1}); (e) CPC total particle count; (f) Left Axis: $\text{PM}_{2.5}$ gravimetric mass with sea salt subtracted, and associated organic and black carbon; Right Axis-dots: Can Carbon Monoxide (ppbv); (g) Left Axis-red: DRUM impactor time series of inferred PM_{1} inferred ammonium sulfate ($\mu\text{g m}^{-3}$); Right Axis-blue: Inferred coarse mode sea salt ($d_p > 0.8 \mu\text{m}$). (h) NAAPS total fine mode particle mass segregated into Anthropogenic (+Biogenic) fine mode and biomass burning.

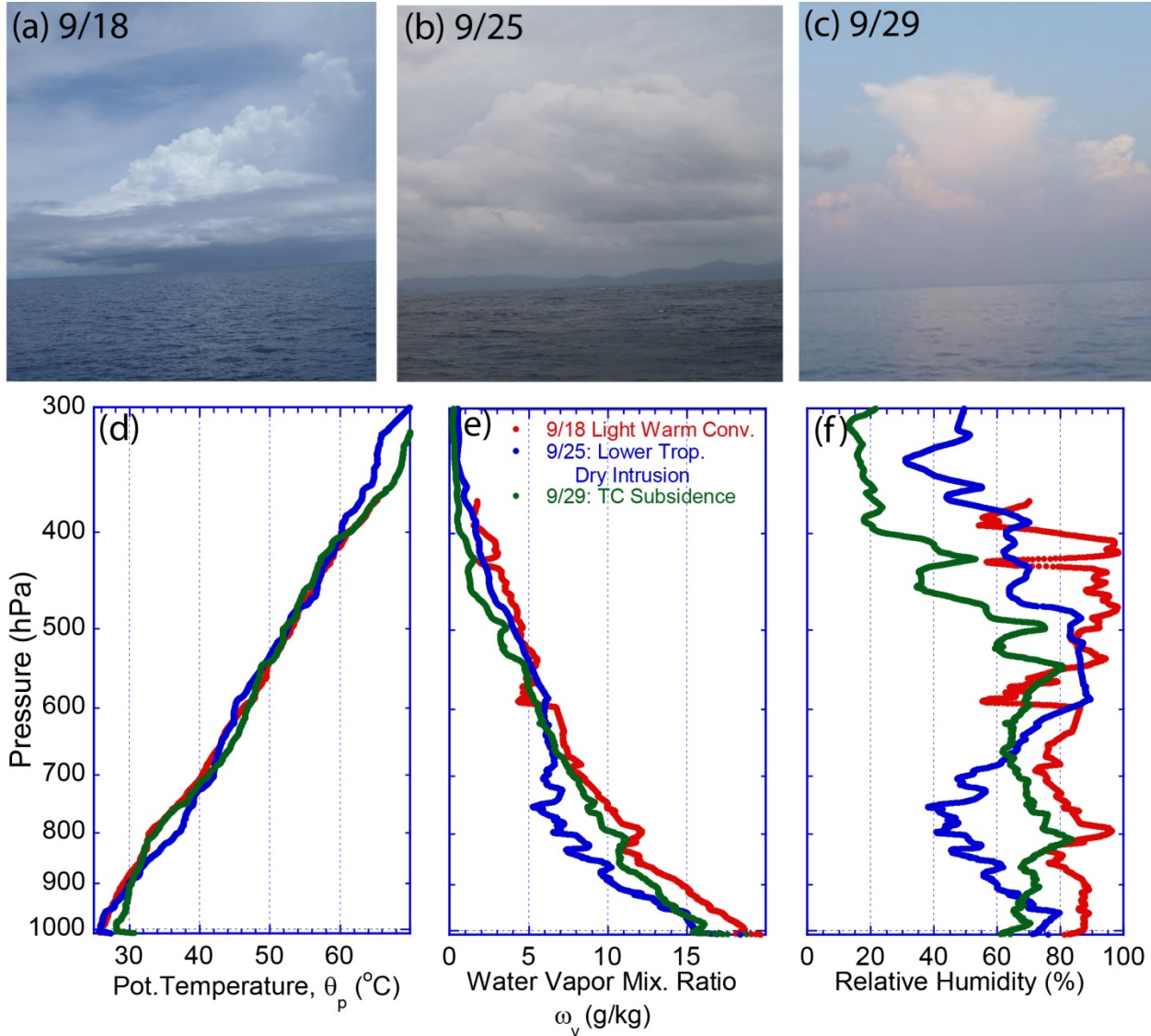


Figure 8. Photographs and corresponding sounding elements for three aerosol regimes during periods of marginal convection. a) Sept. 18th at Apo reef with isolated warm convection in moderately moist conditions; (b) Sept 25th at El Nido with warm non precipitating convection with a lower troposphere dry intrusion during the height of the pollution event; (c) Sept. 29th at the Northern Sulu Sea with isolated deep convection in overall TC induced subsidence during height of biomass burning event. (d), (e) and (f) Corresponding *Vasco* released radiosonde profiles of potential temperature, water vapor mixing ratio, and relative humidity, respectively.

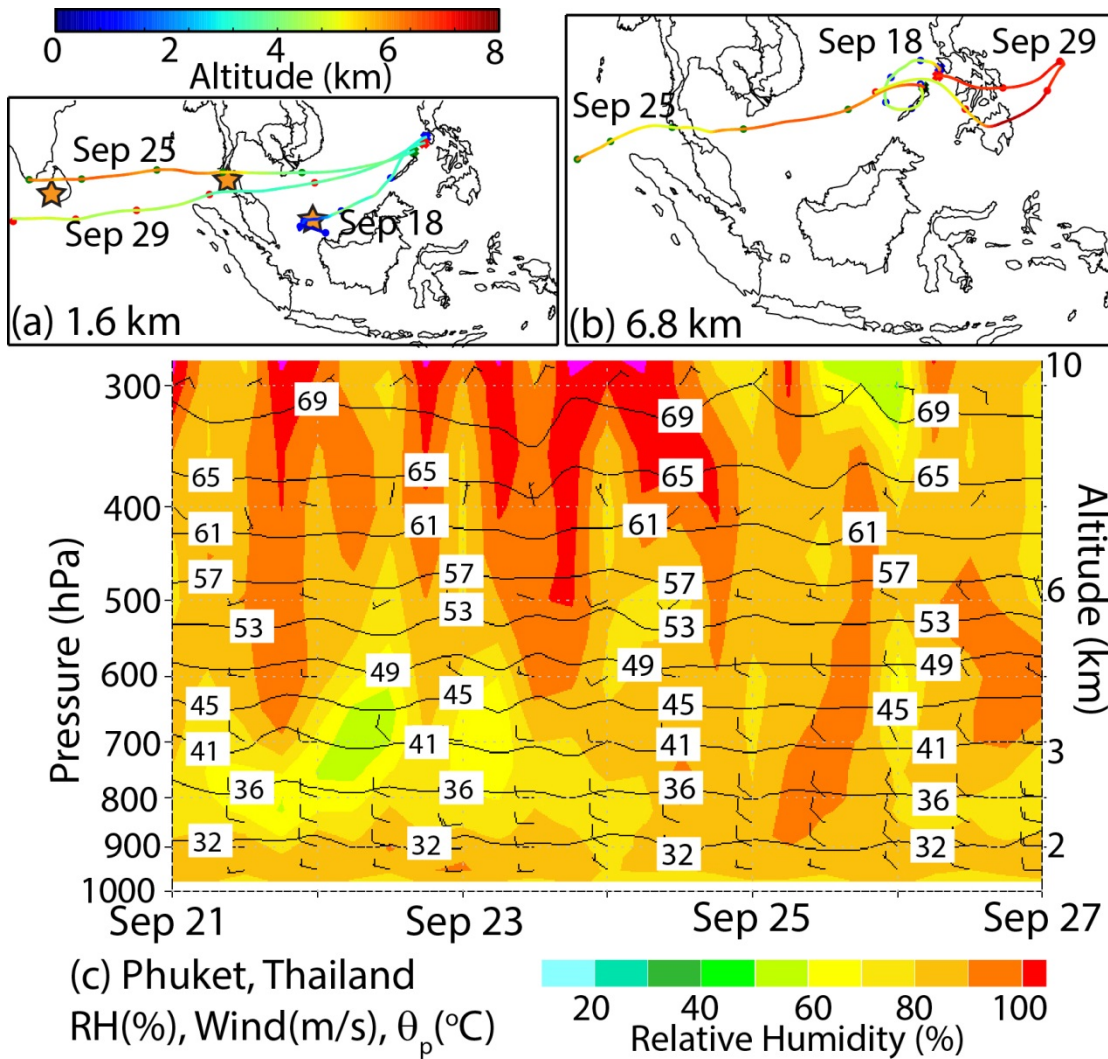


Figure 9. Back trajectories and time height cross sections. (a) & (b) 1.6 km and 6.8 km back trajectories from the *Vasco* for the cases posted in Figure 11. (c) Time height cross section for Phuket, Thailand, of relative humidity-color (RH) with potential temperature isopleths ($^{\circ}\text{C}$). Wind barbs are given with full and half bar at 10 and 5 m/s, respectively.

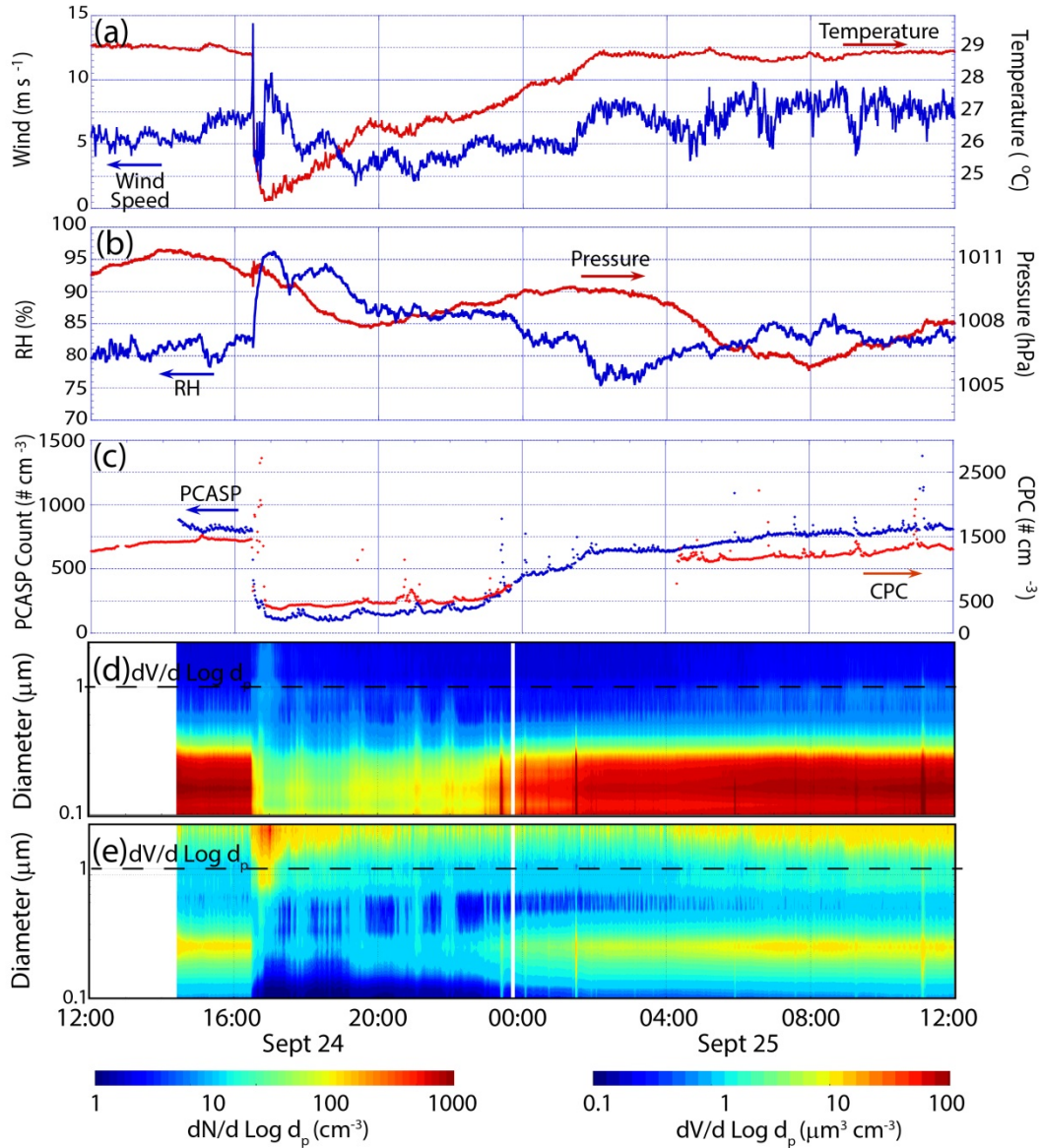


Figure 10. Twenty four hour times series of meteorology and aerosol parameters centered on the September 24th cold pool event. Times are in UTC. (a) 1 minute temperature and wind speed; (b) 1 minute relative humidity and pressure; (c) PCASP and CPC total aerosol particle count; (d) and (e) PCASP number and volume distributions, respectively.

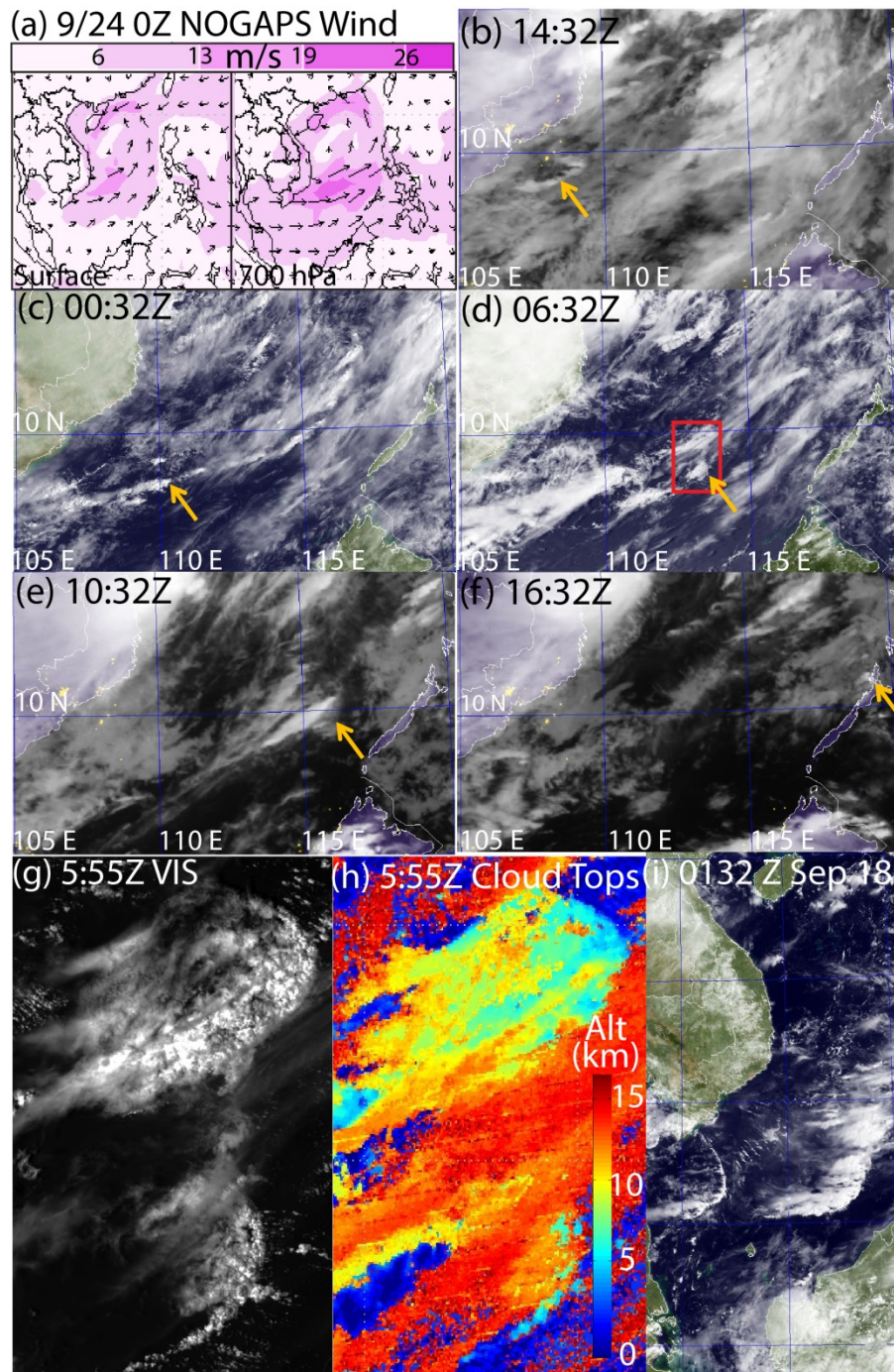


Figure 11. Day visible and night infrared time series of September 24th squall line/cold pool event. (a) Sept 24th 0Z NOGAPS surface and 700 hPa winds at event initiation. (b) Sept. 23rd 14:32Z cold pool arc cloud propagating south from Ho Chi Min City initiated thunderstorm. (c) Sept 24th 00:32Z, convective cell spawned by cold pool, propagating to the NNE; (d) Sept 24th 06:32 Z cold pool from cell in (c); (e) Convective cell spawned by cell in (e); (f) final cell spawned by cold pool from (e) sampled by *Vasco.*; (g) & (h) 250 m MODIS Aqua Ch 1 visible and derived cloud height product respectively. Inset in (d) is the domain. (i) Sep 18 0132 Z MTSAT image of extensive latitudinal dimension of two squall line events.

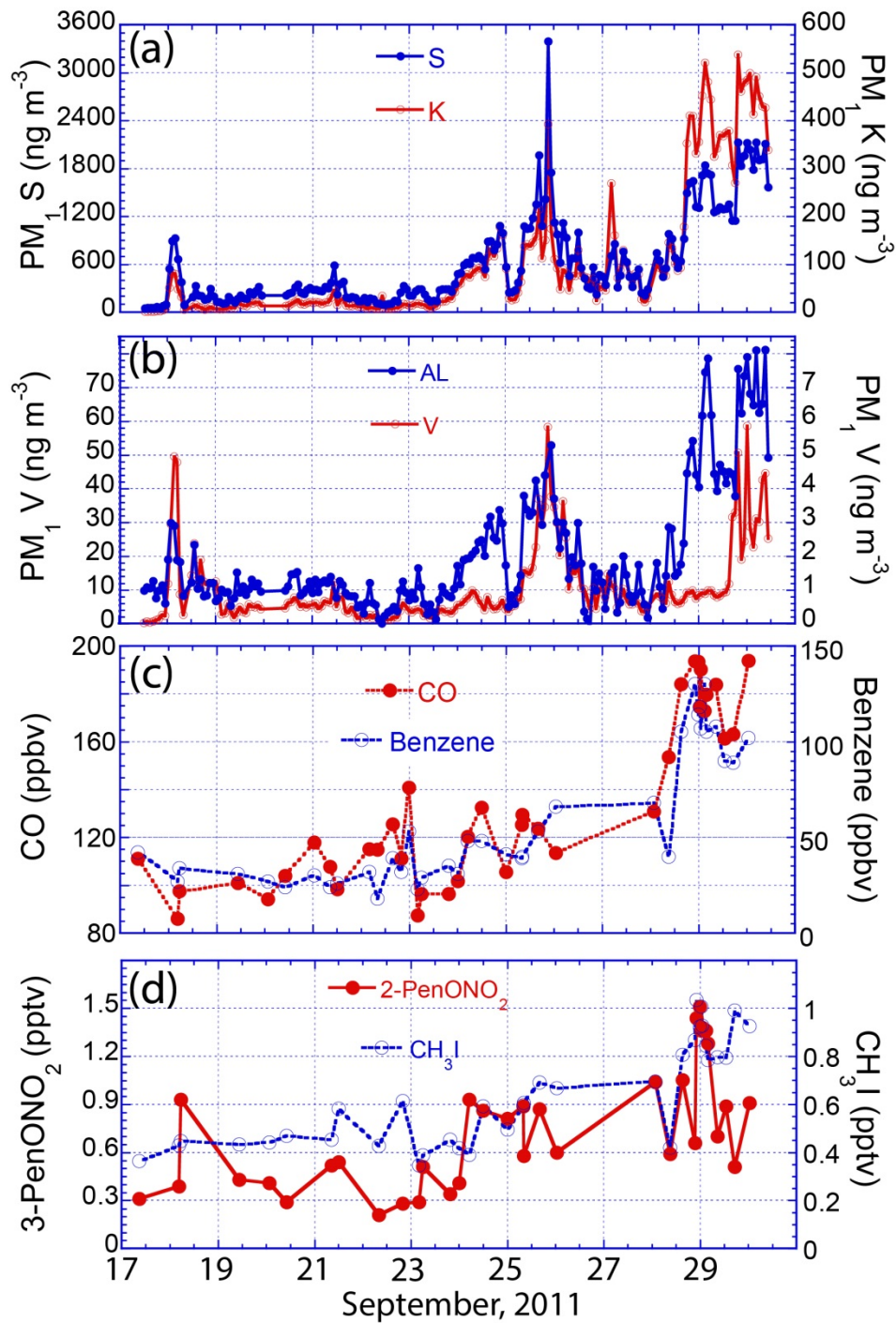


Figure 12. Time series of (key elements and gases. (a) & (b) DRUM time series of Sulfur + Potassium & Aluminum + Vanadium, respectively. (c) Carbon Monoxide and Benzene, both common biomass burning emissions. (d) 2-Pentane Oxyl Nitrate, a photochemical pentane daughter product and Methyl-Iodide, a halogenated organic species also emitted by burning, the oceans, and used in agriculture.

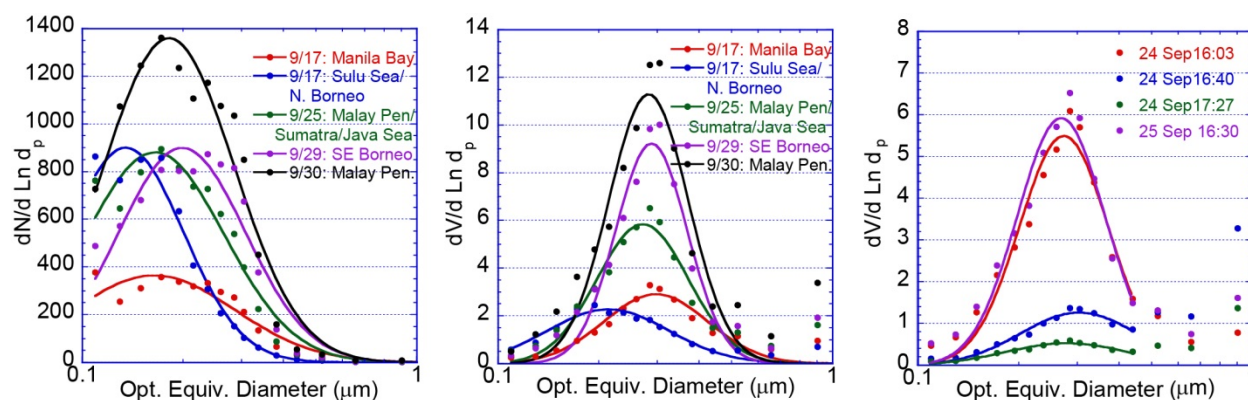


Figure 13. PCASP size distributions for selected regimes. (a) & (b) Number and volume distributions for early, middle and late cruise periods. (c) Volume distributions corresponding to the Sept 24th cold pool event.